Symposium

Nanoparticles and Nanomaterials

Book of Abstracts

Venice, Italy
June 4 – 5, 2026

NPNM Venice June 4 – 5 2026

NP PT

UNIVERSITÄT DUISBURG ESSEN
Open-Minded

Program Overview

Thursday, June 4, 2026

08:40	**Opening address**	Markus Winterer
	Interfaces, properties and applications	chair: Wolf
08:50	**Joachim Maier, MPI Stuttgart**	
09:30	**Vladimir Srdić, U Novi Sad**	
09:50	**Bilge Yildiz, MIT**	
	Soft matter and medical applications	chair: Pratsinis
11:00	**Katja Siebecke, UDE**	
11:20	**Umberto Anselmi-Tamburini, U Pavia**	
11:40	**Sarbari Bhattacharya, Bangalore U**	
12:00	**Frank Menzel, Evonik**	
14:00	***Poster Session***	chairs: Anselmi-Tamburini, Wolf, Winterer
	Optical Properties	chair: Yildiz
15:00	**Emory Chan, LBL**	
15:40	**Gerd Bacher, UDE**	
16:00	**Wayne Gladfelter, U Minnesota**	
16:20	**André Schleife, UIUC**	
	2D Materials	chair: Anselmi-Tamburini
17:30	**Luna Patali Maffei, Politecnico di Milano**	
17:50	**Marika Schleberger, UDE**	
18:10	**Tilmar Kümmell, UDE**	
18:30	**Franziska Münzer, UDE**	
18:50	**Conclusion**	

Friday, June 5, 2026

	Characterization methods	chair: Winterer
08:20	**Julie Villanova, ESRF**	
09:00	**Shradha R. Joshi, UDE**	
09:20	**Martin A. Schroer, UDE**	
09:40	**Janusz Fidelus, GUM**	
	Gas phase processes and films	chair: Winterer
10:30	**Sotiris E. Pratsinis, ETH Zürich**	
10:50	**Burak Atakan, UDE**	
11:10	**Felipe Morgado, UDE**	
11:30	**Nicolas Wöhrl, UDE**	
11:50	**Axel Lorke, UDE**	
	Gas phase processes and nanoparticles	chair: Pratsinis
13:30	**Adam Boies, Stanford U**	
14:10	**Christof Schulz, UDE**	
14:30	**Hartmut Wiggers, UDE**	
14.50	**Einar Kruis, UDE**	
	Sintering	chair: Anselmi-Tamburini
15:30	**Richard Todd, U Oxford**	
16:10	**Jeldrik Schulte, UDE**	
16:30	**Dietrich Wolf, UDE**	
16:50	**Oliver Diwald, Paris-Lodron U Salzburg**	
	Nanocrystalline Materials	chair: Wolf
17:30	**Christopher Schuh, Northwestern U**	
18:10	**Subramshu Bhattacharya, IIT Madras**	
18:30	**Conclusion:** Anselmi-Tamburini, Wolf, Winterer	
19:30	***Conference Dinner***	

Front Cover Legend / Acknowledgement
The false colored SEM images in the front cover display nanocrystalline In_2O_3 before (green body, left) and after sintering (right) courtesy of MSc Jeldrik Schulte (NPPT, UDE).

Symposium

Nanoparticles and Nanomaterials

Venice, Italy, June 4 – 5, 2026

International Advisory Board

Horst Hahn, The University of Arizona, Tuscon, USA and KIT, Germany
Sotiris E. Pratsinis, ETH Zurich, Switzerland
Bilge Yildiz, Massachusetts Institute of Technology, MIT, USA

Local Organizing Committee

Markus Winterer, University of Duisburg-Essen, Germany
Umberto Anselmi-Tamburini, Università di Pavia, Italy
Dietrich Wolf, University of Duisburg-Essen, Germany

Conference Secretary

Sabine Deimel
mail: npnm@web.de
phone: +49-203-379-4445
fax: +49-203-379-4453

Web-page

https://npnm.info

Venue

Venice International University on San Servolo in Venice, Italy

Symposium Nanoparticles and Nanomaterials

NPNM, the international Symposium on Nanoparticles and Nanomaterials covers theoretical and experimental advances regarding synthesis, processing, characterization, properties and applications of nanoparticles and nanomaterials.

June 2026

The organizing committee

Markus Winterer, University of Duisburg-Essen
Umberto Anselmi-Tamburini, Università di Pavia
Dietrich Wolf, University of Duisburg-Essen

Contents

Abstracts continued

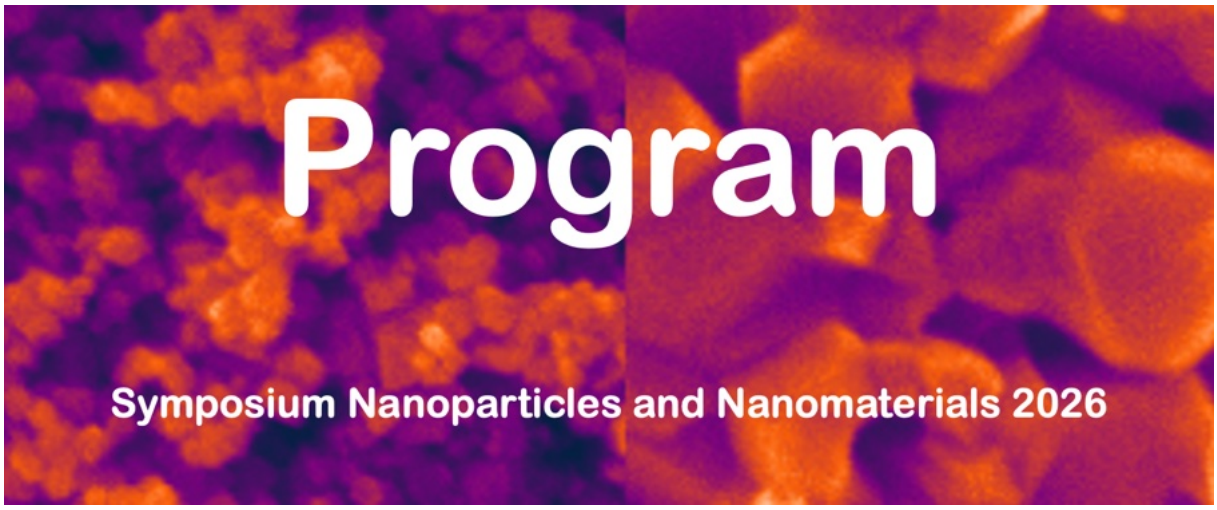
Program
Symposium Nanoparticles and Nanomaterials 2026

Symposium Nanoparticles and Nanomaterials, Venice 2026

Thursday, June 4th – morning –		
08:00	Registration	
08:40	Opening address	Winterer
	Interfaces, properties and applications	Chair: Wolf
08:50	Nanoionics: transport and storage	Maier, MPI Stuttgart
09:30	Ferroelectric field effect transistors based on $(Ba,Sr)TiO_3/(La,Sr)MnO_3$ epitaxial heterostructures prepared by solution deposition technique	Srdic, U Novi Sad
09:50	Controlling nanoparticle catalyst exsolution on oxides – role of defects and surface chemistry	Yildiz, MIT
10:30	Coffee break	
	Soft matter and medical applications	Chair: Pratsinis
11:00	Perfluorocarbon-based artificial oxygen carriers: nanoemulsion and nanocapsules to support life	Siebecke, UDE
11:20	Nanoparticle-cell interactions: from fundamental mechanisms to cancer treatments	Anselmi-Tamburini, U Pavia
11:40	Combining optical traps and ferrofluids to probe magnetic and thermal inhomogenities in microenvironment	Sarbari Bhattacharya, Bangalore U
12:00	Adhesion at the nanoscale: engineering dry-coated silicon anodes for advanced lithium-ion batteries	Menzel, Evonik
12:20	Lunch break	

Symposium Nanoparticles and Nanomaterials, Venice 2026

Thursday, June 4th – afternoon –		
14:00	**Poster session** (posters may stay up during the whole symposium)	Chairs: Anselmi-Tamburini, Winterer and Wolf
1	Surface-enhanced decomposition of $Al(acac)_3$ in MOCVD	Adaköy, UDE
2	Toward inhalation-relevant in vitro exposure: aerosol-dased delivery of nanoparticles at the air-liquid interface	Menzel, Evonik
3	Robotic synthesis and machine-learning-guided optimization of complex upconverting nanoparticle heterostructures	Peterschik, UDE
4	From the microscale to the macroscale: kinetic modelling of carbon particles and carbon deposition from methane pyrolysis	Pratali Maffei, Politecnico di Milano
5	In situ dynamic light scattering during the ultrasonication of nanoparticle dispersions	Rahtz, UDE
6	Preparation of polyacrylonitrile-based carbon nanofibers and their applications in energy storage and conversion technologies	Shin, DTNW
7	Nanocrystalline CoMnFeNiGa high-entropy alloys across length scales: processing-driven structure and magnetism	Shkodich, UDE
8	Designing a modular chemical vapor synthesis reactor for in situ X-ray scattering and spectroscopy	Stepponat, UDE
9	Entropy-stabilized $LaMnO_3$ based thin films obtained by PAD: structure and transport properties	Vukmirovic, U Novi Sad
	Optical properties	Chair: Yildiz
15:00	Photon avalanching nanoparticles	Emory Chan, LBL
15:40	Interparticle and intraparticle energy transfer in doped CdSe nanocrystals	Bacher, UDE
16:00	Indium oxide nanocrystals as excited state electron acceptors	Gladfelter, U Minnesota
16:20	First-principles modeling of optoelectronic properties and strain engineering in II-VI chalcogenide alloys and core-shell nanostructures	Schleife, UIUC
17:00	Coffee break	
	2D Materials	Chair: Anselmi-Tamburini
17:30	Rationalizing quantum-dot behavior in flame-formed carbon nanoparticles: from accurate excitation energies to stacking effects	Pratali Maffei, Politecnico di Milano
17:50	2D semiconductors: defects, interfaces, and new opportunities	Schleberger, UDE
18:10	Optical monitoring of substrate doping in MOCVD grown MoS_2 monolayers	Kümmell, UDE
18:30	Grain-boundary states enable charge separation and narrow-band photoresponse in 2D perovskites	Münzer, UDE
18:50	**Conclusion**	Anselmi-Tamburini, Wolf, Winterer
Informal dinner		

Symposium Nanoparticles and Nanomaterials, Venice 2026

Friday, June 5th – morning –		
	Characterization methods	Chair: Winterer
08:20	Synchrotron X-ray nano-analysis & imaging	Villanova, ESRF
09:00	Observing the evolution of nanocrystals by in situ and operando X-ray diffraction during chemical vapor synthesis	Joshi, UDE
09:20	Deciphering the agglomerate structure of nanoparticle dispersions for medical applications by X-ray scattering	Schroer, UDE
09:40	Silicon-based nanostructured calibration standards for traceable scanning probe microscopy	Fidelus, GUM
10:00	Coffee break	
	Gas phase processes and films	Chair: Winterer
10:30	The diffusivity of tiny nanoparticles in the gas phase	Pratsinis, ETH Zürich
10:50	Mass spectrometric investigation of gas phase reactions of Aluminium acetylacetonate with water and oxygen	Atakan, UDE
11:10	Pulsed precursor flow in chemical vapor synthesis and deposition of oxides as nanocrystals and epitaxial thin films	Morgado, UDE
11:30	Formation of coral-like nanostructures on nickel surfaces via remote nitrogen plasma treatment	Wöhrl, UDE
11:50	Plasma-induced optically active defects in the van-der-Waals material hBN (hexagonal boron nitride)	Lorke, UDE
12:10	Lunch break	

Symposium Nanoparticles and Nanomaterials, Venice 2026

Friday, June 5th – afternoon –		
	Gas phase processes and nanoparticles	Chair: Pratsinis
13:30	Aerosol CNT synthesis at scale – what is needed for kilotonne to megatonne production?	Boies, Stanford U
14:10	Formation of free-standing graphene in microwave plasma synthesis	Schulz, UDE
14:30	Spray-flame synthesis of inorganic multi-element oxides	Wiggers, UDE
14:50	Real-time control of nanoparticle synthesis by spark ablation	Kruis, UDE
15:10	Coffee Break	
	Sintering	Chair: Anselmi-Tamburini
15:30	Grain boundary development between nanoparticles: evidence from rapid sintering of alumina	Todd, U Oxford
16:10	A time-resolved exploration of resonant laser sintering	Schulte, UDE
16:30	Flash effect on reduction- and oxidation-fronts propagating through TiO_2	Wolf, UDE
16:50	$BaTiO_3$ nanoparticle-derived microstructures: sintering approaches and reactivity	Diwald, Paris-Lodron U Salzburg
17:10	Coffee Break	
	Nanocrystalline materials	Chair: Wolf
17:30	Machine-learned solute segregation spectra and the stability of nanocrystalline materials	Schuh, Northwestern U
18:10	Synthesis, characterization and structure-property correlations in nanostructured multicomponent, equimolar high entropy oxides	Subramshu Bhattacharya, IIT Madras
18:30	**Conclusion**	Anselmi-Tamburini, Wolf, Winterer
Break		
19:30	**Conference dinner**	

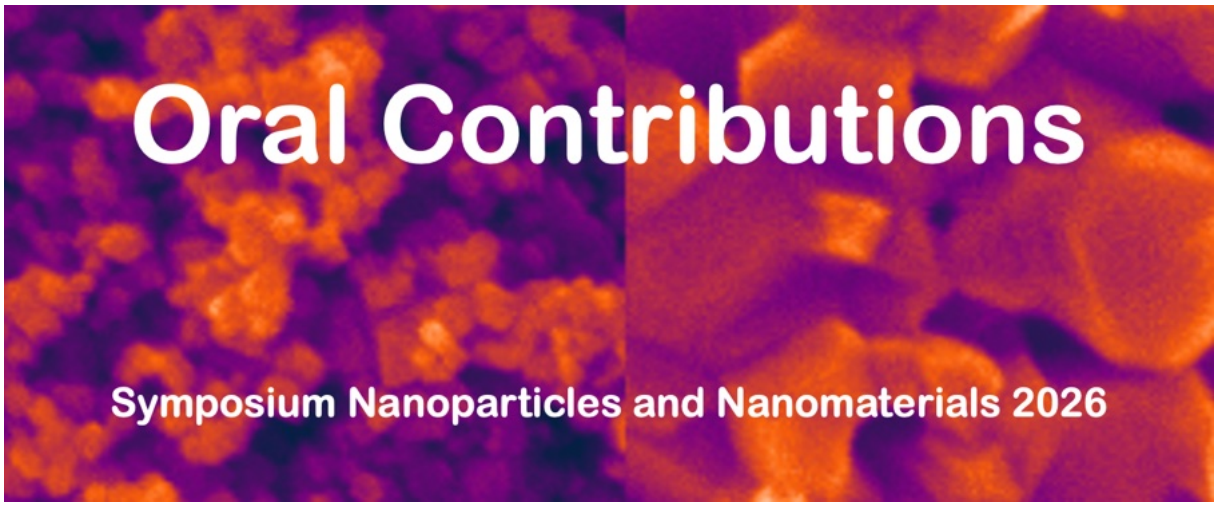

(Abstracts in order of appearance in the oral program; presenting author in **bold)**

Notes

Nanoionics: transport and storage

Joachim Maier

Max Planck Institute for Solid State Research, Physical Chemistry of Solids, Stuttgart, 70569, Germany

The presentation discusses ionic charge carrier effects on the nanoscale [1]. Ion transport is then dominated by space charge effects and can be modulated by size and neighboring phases. A master example is given by solid electrolytes based on heterostructures [2]. Even more exciting is the consideration of transport properties of mixed conductors [3], as here the impact of the chemical environment can be studied.

Of no less relevance are storage effects on the nanoscale. This then not only affects understanding of “storage anomalies” in electrodes for Li- or Na-batteries [4] but even allows for unifying battery and supercapacitor concepts [5].

[1] Maier, J., Nature Materials **4** (2005) 805, doi.org/10.1038/nmat1513.
[2] Sata, N., Eberman, K., Eberl, K., Maier, J., Nature **408** (2000) 946, doi.org/ 10.1038/35050047.
[3] Lupetin, P., Gregori, G., Maier, J., Angew. Chemie Int. Ed. **49** (52) (2010) 10123, doi.org/ 10.1002/anie.201003917.
[4] Maier, J., Angew. Chem. Int. **52** (2013) 4998, doi.org/10.1002/anie.201205569.
[5] Xiao, C., Wang, H., van Aken, P., Usiskin, R., Maier, J., Science **386** (2024) 407, doi.org/10.1126/science.adi5700.

Notes

Ferroelectric field effect transistors based on $(Ba,Sr)TiO_3/(La,Sr)MnO_3$ epitaxial heterostructures prepared by solution deposition technique

Vladimir V. Srdić[1,2], Jelena Vukmirović[1], Danica Piper[3], Iva Toković[1], Xuyun Guo[4], Felipe Morgado[5], Venkatadivakar Botcha[3], and Branimir Bajac[3]

1 Department of Materials Engineering, Faculty of Technology Novi Sad, University of Novi Sad, Bul. Cara Lazara 1, 21000 Novi Sad, Serbia
2 Serbian Academy of Sciences and Arts, Kneza Mihajla 35, 11000 Belgrade, Serbia
3 Institute BioSense, University of Novi Sad, Dr. Zorana Đinđića 1, Novi Sad, Serbia
4 School of Chemistry, Centre for Research on Adaptive Nanostructures and Nanodevices (CRANN) and Advanced Materials Bio-Engineering Research Centre (AMBER), Trinity College Dublin, D02 PN40 Dublin, Ireland
5 Nanoparticle Process Technology, Faculty of Engineering, University Duisburg Essen, Lotharstr. 1, 47057 Duisburg, Germany

Ferroelectric field effect transistor (FeFET), a semiconductor device with a metal ferroelectric-semiconductor structure where the traditional oxide dielectric is replaced by a ferroelectric material, has found variety applications in different fields. The operational principle is based on the manipulation of the polarization direction of the ferroelectric medium by applying a gate voltage. This applied voltage changes the surface state of the semiconductor channel layer and modulates the switching state of the transistor. Polarization control in the ferroelectric devices is usually accomplished by application of an electric field, but for specific applications photo-induced reverse ferroelectric polarization is of great importance. The corresponding device that enhances the interaction between light and material within a confined space might have a variety of applications, including sensor technology, optical communications, etc.

In this paper, we designed FeFET device consisting of ferroelectric barium strontium titanate layer on top of lanthanum manganite based channel, having printed gate, source and drain. Bilayer epitaxial thin film heterostructures based on $La_xSr_{1-x}MnO_3$ (LSMO) and $Ba_xSr_{1-x}TiO_3$ (BSTO) were fabricated using a solution-based approach. For LSMO, precursor solutions were prepared by dissolving metal nitrates in distilled water, where PEI and EDTA polymers were employed to keep precursor ions coordinated and to prevent the early formation of undesirable phases. Prepared solutions were spin coated to obtain single layers on the $SrTiO_3$ single crystal substrate. Deposited layers were thermally treated at temperatures up to 900°C to obtain LSMO epitaxial thin film with approximate thickness ~10 nm. In the next step, part of the LSMO surface was covered by BSTO layer, prepared by sol-gel method in combination with spin coating. The deposited layers were thermally treated at temperatures up to 900°C to obtain epitaxial BSTO thin film with approximate thickness ~10 nm. Finally, gold electrodes were deposited by electron-beam physical vapor deposition method. Structure and electrical properties of the fabricated devices were investigated.

Notes

Controlling nanoparticle catalyst exsolution on oxides – role of defects and surface chemistry

Bilge Yildiz

Department of Nuclear Science and Engineering and Department of Materials Science and Engineering, Massachusetts Institute of Technology, 77 Massachusetts Avenue, 24-210 Cambridge, MA 02139, USA

Exsolution is an effective approach to fabricating oxide-supported metal nanoparticle catalysts via phase precipitation out of a host oxide. A fundamental understanding and control of the exsolution kinetics are needed to engineer exsolved nanoparticles to obtain higher catalytic activity toward clean energy and fuel conversion. Since oxygen release via oxygen vacancy formation in the host oxide is behind oxide reduction and metal exsolution, we hypothesize that the kinetics of metal exsolution should depend on the kinetics of oxygen release and the resulting oxygen vacancies at the surface. In this work, we probe the surface exsolution kinetics both experimentally and theoretically using thin-film perovskite oxide model systems, show its relation to the oxygen evolution kinetics, and tune it by external drivers including elastic strain and ion irradiation. Using both drivers, we couple to the formation of point defects and defect clusters, that serve as nucleation sites for nanoparticle exsolution on epitaxial perovskite oxides. Lastly, we modify the surface chemistry by reducible and volatile layers to exsolve highly active alloy nanoparticles that remain more stable at elevated temperatures. As a result, we can controllably tune size, density, composition and position of the exsolved metal nanoparticles.

Notes

Perfluorocarbon-based artificial oxygen carriers: nano-emulsion and nanocapsules to support life

Katja B. Siebecke née Ferenz[1,4], Jan-Eric Sydow[2], Fabian Nocke[2], and Martin A. Schroer[3,4]

1 Institute of Physiology, University of Duisburg-Essen, University Hospital Essen, 45147 Essen, Germany
2 Institute of Physiological Chemistry, University of Duisburg-Essen, University Hospital Essen, 45147 Essen, Germany
3 Nanoparticle Process Technology (NPPT), Faculty of Engineering, University of Duisburg-Essen, 45057 Duisburg, Germany
4 CeNIDE, University of Duisburg-Essen, 45057 Duisburg, Germany

Thanks to their immediate availability, blood group independence and durability, perfluorocarbon-based artificial oxygen carriers (AOCs) represent an attractive alternative to red blood cell concentrates in many areas. Due to the cavities between the individual molecules, perfluorocarbons exhibit a high solubility for respiratory gases compared to aqueous media and can therefore take over O_2 transport instead of red blood cells or even support them in cooperation [1]. We have already demonstrated this in isolated perfused organs [2-4] and in vivo [5-6] for our albumin-derived perfluorocarbon-based artificial oxygen carriers. In order to offer a perfluorocarbon-based oxygen carrier that is optimally tailored to the needs of a wide range of applications (such as blood replacement, machine perfusion of organs or cell cultures), we now have different subtypes of our perfluorocarbon-based oxygen carrier in our actual portfolio.

We developed two subtypes with improved stability in clinically used carrier solutions. For this we (i) modified the shell of the oxygen carrier via biocompatible cross-linking with glucose resulting in nanocapsules, named G-AOCs (glucose-linked artificial oxygen carriers); and (ii) modified the emulsifier composition of the original nanoemulsion by mixing a second emulsifier (lecithin) with albumin creating LENOX (lecithin-modified nanoscale oxygen carriers) [7].

Glucose cross-linking resulted in colloidally stable nanocapsules of long-time stability with only minor loss in oxygen capacity. Structural characterization by solution small angle x-ray scattering (SAXS) revealed a synthesis-dependent particle size distribution, while no structural changes were observed within 5 to 37°C demonstrating their thermal stability.

Addition of lecithin resulted in nanoemulsions with unaffected oxygen capacity and high stability in various clinically relevant media over the storage period of 42 days at 4°C. SAXS measurements reveal structural and colloidal stability against dilution and the absence of agglomeration. Since LENOX are not cytotoxic and now compatible with clinically used media, they are ideally suited to provide oxygen in further in vitro experiments and are promising for in vivo use, e.g., in the context of blood replacement or ex vivo organ machine perfusion prior to transplantation.

[1] Jägers J., Wrobeln A., Ferenz K.B., Pflugers Arch., **473** (2021) 139; doi: 10.1007/s00424-020-02482-2
[2] Jägers J., Kirsch M., Cantore M., Karaman O., Ferenz K.B. Artif., Organs, **46** (2022) 1783; doi: 10.1111/aor.14264
[3] Wrobeln A., Schlüter K.D., Linders J., Mayer C., Ferenz K.B., Artif. Cells Nanomed. Biotechnol, **45** (2017), 723; doi: 10.1080/21691401.2017.1284858
[4] Rother T., Horgby C., Schmalkuche K., Burgmann J.M., Nocke F., Jägers J., Schmitz J., Braesen J.H., Cantore M., Zal F., Ferenz K.B., Blasczyk R., Figueiredo C., Front. Transplant. (2023) 2:1183908; doi: 10.3389/frtra.2023.1183908
[5] Wrobeln A., Jägers J., Quinting T., Schreiber T., Kirsch M., Fandrey J., Ferenz K.B., Sci. Rep., **10** (2020) 11950; doi: 10.1038/s41598-020-68701-z
[6] Wrobeln A., Laudien J., Groß-Heitfeld C., Linders J., Mayer C., Wilde B., Knoll T., Naglav D., Kirsch M., Ferenz K.B., Eur J Pharm Biopharm, **115** (2017) 52; doi: 10.1016/j.ejpb.2017.02.015
[7] Nocke F., Schroer M.A., Penzel M., Cantore M., Steinbicker A.U., Ferenz K.B., Adv. NanoBiomed Res. **5** (2025) 2500117; doi: 10.1002/anbr.202500117

Acknowledgements: We thank Markus Winterer for his continuous support.

Notes

Nanoparticle-cell interactions: from fundamental mechanisms to cancer treatments

Umberto Anselmi-Tamburini[1], Patrizia Sommi[2], Maria Paola Demichelis[3], and Marcella Tazzari[4]

1 Department of Chemistry, University of Pavia, 27100 Pavia, Italy
2 Department of Molecular Medicine, University of Pavia, 27100 Pavia, Italy
3 Unit of Pavia, National Institute of Nuclear Physics, INFN, 27100 Pavia, Italy
4 Advanced Cellular Therapies and Rare Tumors Unit, IRCCS Istituto Romagnolo per lo Studio dei Tumori (IRST) "Dino Amadori", 47014 Meldola, Italy;

Nanoparticles have attracted considerable attention over the past two decades for their potential applications in medical treatment. A wide range of applications has been demonstrated in drug delivery, imaging, and diagnostics, with more advanced applications, such as targeted gene therapy and smart, responsive nanomedicines, still being explored. Despite this extensive research and promising preclinical results, clinical adoption of nanomedicine has been slower than initially anticipated. This is due to several factors, including the difficulty of translating findings from in vitro and animal models to humans, safety concerns, manufacturing and scalability challenges, and unclear regulatory pathways. One main limiting factor, however, is represented by the complexity of interactions between nanoparticles and the biological environment. The interaction of nanoparticles with living organisms is more complex than that of traditional drugs and takes place at different scales. Here, we present examples of how differences in nanoparticle chemical and physicochemical characteristics can influence their interactions with cells and regulate mechanisms of cellular uptake. In particular, we will discuss inorganic nanoparticles, such as CeO_2 nanoparticles (CNPs) [1, 2], and BN quantum dots (BNQDs) [3]. We show that polyacrylic acid-functionalized CNPs interact only with specific structures of the cell's outer membrane, thereby defining a distinctive internalization route into lysosomes [1], the final intracellular destination. Moreover, the interaction with the acidic environment of these structures, rather than their surface characteristics, is fundamental to their antioxidant activity [2]. BNQDs evidenced a very different intracellular distribution and an incorporation mechanism, probably associated to their ultra-small dimension [3].

Another factor that has limited the widespread application of nanomedicine is the clearance challenge. When introduced in living organisms, nanoparticles undergo rapid opsonization and uptake by the mononuclear phagocyte system. As a result, nanomedicines that perform well in vitro are rapidly removed or inactivated in vivo, preventing sufficient target accumulation and hampering their successful translation into clinical practice. To overcome this limitation, we developed an approach using circulating cells, specifically T lymphocytes, as "Trojan horses" that can be tailored to each patient's tumor. In a proof-of-concept study, we demonstrated that T cells isolated from oncological patients can load significant amounts of composite nanostructures composed of B_4C and Fe_2O_3 (FeBNC) [4]. These nanostructures exhibit theragnostic properties, serving as a source of ^{10}B for boron neutron capture therapy (BNCT) applications, while their distribution can be imaged using MRI techniques. This approach could provide a platform for targeted drug delivery, improving targeting and penetration compared with traditional methods.

[1] Sommi, P., Vitali, A., Coniglio, S., Callegari, D., Barbieri, S., Casu, A., Falqui, A., Vigano', L., Vigani, B., Ferrari, F. and Anselmi-Tamburini, U., ACS Nano, **15** (2021) 15803. https://doi.org/10.1021/acsnano.1c03151
[2] Sommi, P., Callegari, D., Ferraro, D., Ghigna, P., Castillo-Michel, H., Viganò, L., Vitali, A., Fracchia, M., Falqui, A., Demichelis, M.P. and Profumo, A., ACS Applied Materials & Interfaces **17**, (2025) 22474. https://doi.org/10.1021/acsami.5c02505
[3] Demichelis, M.P., Portu, A.M., Gadan M.A., Sommi P., Milanese C., Falqui A., Bortolussi S., Anselmi-Tamburini U., in preparation.
[4] Demichelis, M.P., Sommi, P., Romanini, N., Portu, A., Gadan, M., Bortolussi, S., Postuma, I., Casu, A., Falqui, A., Palamà, M.E.F. and Scaglione, S., ACS nano, **19** (2025), 42158. https://doi.org/10.1021/acsnano.5c12640

Notes

Combining optical traps and ferrofluids to probe magnetic and thermal inhomogenities in microenvironment

Shruthi S. Iyengar[1,2] and **Sarbari Bhattacharya**[1]

1 Department of Physics, Bangalore University, Bangalore 560056, India
2 Raman Research Institute, Bangalore 560080, India

Optically trapped microbeads serve as sensitive probes of their local environment. When suspended nanoparticles are introduced into the fluid surrounding a trapped microbead, the corner frequency in the plane perpendicular to beam propagation direction exhibits isotropic enhancement due to directed particle motion towards the trap [1]. This phenomenon enables detection of physical and chemical changes in the local environment through analysis of the trapping characteristics [2]. By employing ferrofluids (magnetic nanoparticles), the detection of external magnetic fields becomes possible as the isotropic enhancement becomes anisotropic [1]. Furthermore, the presence of magnetic micro entities in the surrounding fluid (fig. 1(a)) as well as their dynamics under external magnetic fields (fig. 1(b)) can be deduced from analysing alterations in the trapping characteristics. When the trap itself contains a magnetic core-shell microbead, localized heating generates thermal gradients in the surrounding medium, enabling the study of nanoparticle dynamics under combined magnetic field and thermal gradients. We thus demonstrate that coupling optically trapped microprobes with nanoparticle suspensions serves as a versatile platform for characterizing complex micro-environments.

[1] Iyengar, S.S., Praveen, P., Ananthamurthy, S. and Bhattacharya, S., App. Opt., **59** (2020) 5114 doi.org/10.1364/AO.389500
[2] Iyengar, S.S. and Bhattacharya, S., Macromol. Symp. **413** (2024) 2300027 doi.org/10.1002/masy.202300027

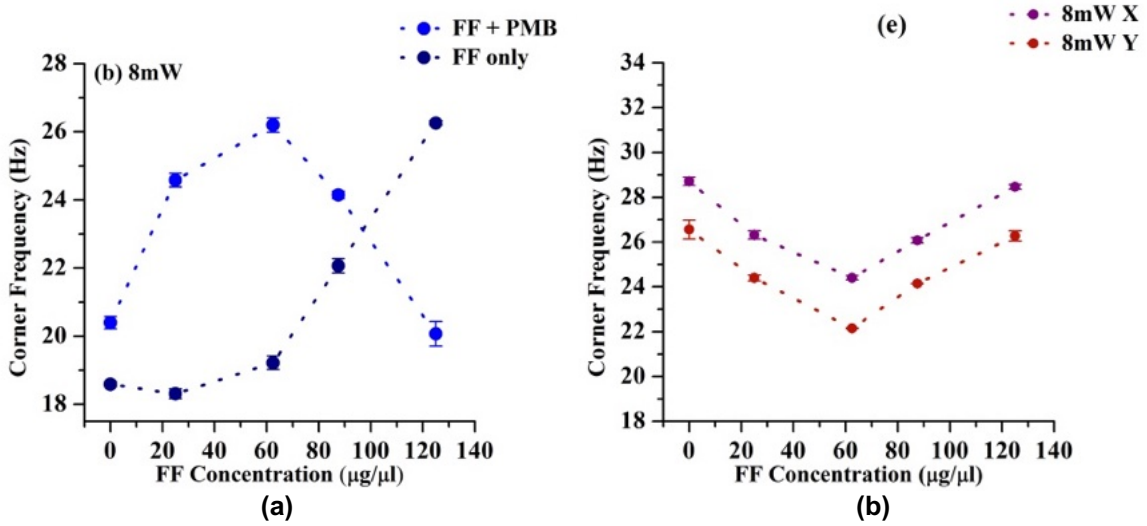

Fig. 1: Variation of corner frequency of an optically trapped non magnetic microbead in the presence of polystyrene magnetite composite microbeads (PMB) as a function of ferrofluid (FF) concentration in (a) absence of external magnetic field and (b) presence of external magnetic field. Anisotropy of the trapping characteristics in the X and Y directions can be clearly seen in the case where the external magnetic field is present. The power of the laser in the plane of trapping is 8mW.

Notes

Adhesion at the nanoscale: engineering dry-coated silicon anodes for advanced lithium-ion batteries

Frank Menzel[1], Ana Luísa Azevedo Costa[1,2], Tatiana Gambaryan-Roisman[2], and Daniel Esken[1]

1 Evonik Operations GmbH, EQR Smart Effects, 63457 Hanau, Germany
2 Institute for Technical Thermodynamics, Technical University Darmstadt, Peter-Grünberg-Straße 10, 64287 Darmstadt, Germany

Nanoparticle strong adhesion interactions often lead to agglomeration, negatively impacting dispersion, functionality, and integration into complex systems. This presentation will explore the mechanisms underlying nanoparticle adhesion, detachment, and surface modification, with a focus on dry particle coating – a scalable, solvent-free technique for tailoring interfacial properties.

Experimental and theoretical studies, including atomic force microscopy (AFM), were conducted to characterize the effects of particle size, surface chemistry, stiffness, and wettability on adhesion and deagglomeration. A modified stick-bounce model was developed to quantify coating quality and predict detachment under varying stress conditions, providing a robust framework for assessing coating performance across diverse materials [1].

Building upon these insights, the dry coating strategy was applied to address a critical challenge in energy storage: stabilizing silicon-based anodes in lithium-ion batteries (LIBs). Silicon, with its high theoretical capacity, suffers from mechanical degradation and unstable interfacial chemistry during electrochemical cycling. To overcome these limitations, nanostructured metal oxide coatings (Al_2O_3, TiO_2, MgO, ZrO_2, SnO_2, and Li_3BO_3) were applied to SiOx/C anodes using the dry coating process (**Fig. 1**). The study investigates the influence of coating particle properties, surface wettability, and morphology on electrode performance, spanning powder processing, electrode fabrication, full cell assembly, and electrochemical testing [2].

Results demonstrate improved structural integrity, stabilized electrolyte interactions, and enhanced cycling performance in silicon-based anodes (**Fig. 2**). Furthermore, investigations into slurry rheology and electrolyte drop impact behavior underscore the importance of nanoscale interfacial engineering in bridging fundamental nanoparticle science with real-world battery manufacturing and operation [3].

This research provides new insights into nanoparticle adhesion and interface phenomena across multiple scales, offering a versatile coating strategy for enhancing material performance in energy storage and other applications where nanoparticle behavior and surface engineering are critical.

This work was supported by the European Union's Horizon 2020 research and innovation program under the Marie Skłodowska-Curie grant agreement No. 955612, through the nanoPaInt project.

[1] Azevedo Costa, A.L., Esken, D., Gambaryan-Roisman, T., Menzel, F., Applied Surface Science **706** (2025) 163401, DOI: 10.1016/j.apsusc.2025.163401
[2] Azevedo Costa, A. L., Liebertseder, M., Gambaryan-Roisman, T., Esken, D., Menzel, F., Electrochemistry Communications **177** (2025) 107941, DOI: 10.1016/j.elecom.2025.107941
[3] Azevedo Costa, A. L., Esken, D., Gambaryan-Roisman, T., Menzel, F. ChemistryOpen **14** (2025) e202500170, DOI.org/10.1002/open.202500170

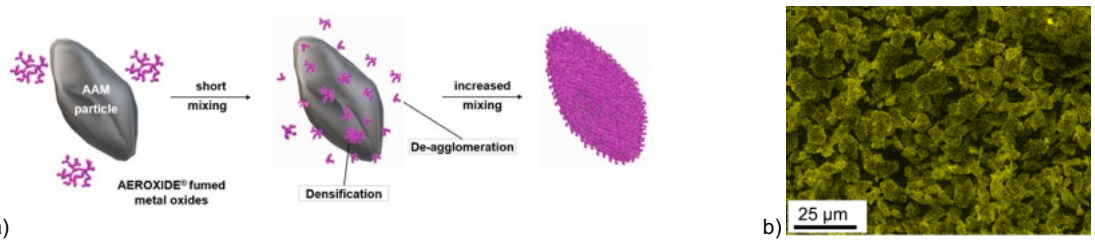

a) b)

Fig. 1: Dry coating process a) scheme and b) SEM image of Al_2O_3-coated anode material

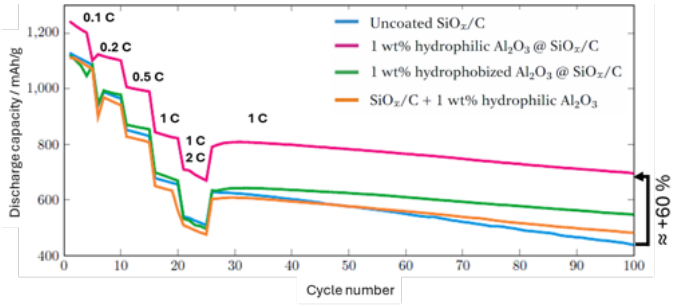

Fig. 2: Effect of Surface Modification on Cycling Performance

Notes

Photon avalanching nanoparticles

Emory M. Chan

The Molecular Foundry, Lawrence Berkeley National Laboratory, Berkeley, California 94720, United States

Lanthanide-doped nanomaterials exhibit nonlinear photophysical dynamics that give rise to photon upconversion, which can be leveraged for applications in optoelectronics, super-resolution imaging, and optical computing. I will discuss the high-throughput discovery and application of a new class of upconverting nanoparticles known as photon avalanching nanoparticles (ANPs). We demonstrate that robotically synthesized thulium-doped $NaYF_4$ nanocrystals excited with 1064 nm light can undergo a unique photon avalanching mechanism that gives rise to giant nonlinear optical responses.[1] These high nonlinearities, equivalent to those of >30-photon processes, enable NIR imaging with <70 nm resolution using only a standard confocal microscope.[1] Furthermore, photon avalanching at high excitation powers facilitates indefinite NIR photoswitching that allows for a second mode of sub-diffraction imaging, based on stochastic localization microscopy (e.g., PALM, STORM), that can achieve < 1 Å localization accuracies.[2]

To expand the library of ANPs, we developed a second type of ANP based on low phonon energy potassium lead halide hosts, whose monodisperse synthesis was achieved by tuning the reactivity of halide precursors.[3] We demonstrate that neodymium-doped KPb_2Cl_5 ANPs can achieve >200^{th}-order nonlinearities and exhibit luminescence hysteresis characteristic of intrinsic optical bistability.[4] Modeling reveals that this purely optical and intrinsic bistability originates from the low phonon energy of the KPb_2Cl_5 host and from the positive feedback of photon avalanching in the Nd^{3+} dopants. The ability to efficiently switch ANP luminescence via IOB allows us to demonstrate high-contrast, transistor-like optical behavior that establishes the potential application of ANPs in optical logic, memory, and computing.

Finally, we will discuss how we use kinetic Monte Carlo and machine learning approaches [5] such as physics-informed graph neural networks to enable rapid inverse design of upconverting nanoparticles, [6] particularly complex heterostructures that exhibit emergent properties such as photon avalanching.

[1] Lee, C. et al. Nature, **589** (2021), 230; https://doi.org/10.1038/s41586-020-03092-9.
[2] Lee, C. et al. Nature, **618** (2023), 951; https://doi.org/10.1038/s41586-023-06076-7.
[3] Zhang, Z. et al. Angew. Chem. Int. Ed., **62** (2023), e202212549; https://doi.org/10.1002/anie.202212549.
[4] Skripka, A. et al. Nat. Photonics, **19** (2025), 212; https://doi.org/10.1038/s41566-024-01577-x.
[5] Xia, X., et al. Nano Lett., **23** (2023), 11129; https://doi.org/10.1021/acs.nanolett.3c03568.
[6] Sivonxay, E. et al. Nature Computational Science (2025); https://doi.org/10.1038/s43588-025-00917-3.

Notes

Interparticle and intraparticle energy transfer in doped CdSe nanocrystals

Gerd Bacher[1], J. Bieniek[1], M. Riesner[1], J. Klein[1], F. von Toperczer[1], F. Shabani[2], L. Zeylmans van Emmichoven[1], S. Delikanli[2], H.V. Demir[2], E. Drescher[3], T. Steenbock[3], G. Bester[3], W. Baek[4], and T. Hyeon[4]

1 Werkstoffe der Elektrotechnik and CENIDE, University Duisburg-Essen, 47057 Duisburg, Germany
2 Department of Electrical and Electronics Engineering, Department of Physics, UNAM-Institute of Materials Science and Nanotechnology and National Nanotechnology Research Center, Bilkent University, Ankara, 06800, Turkey
3 Department of Chemistry, University of Hamburg, 22761 Hamburg, Germany
4 School of Chemical and Biological Engineering and Institute of Chemical Processes, Seoul National University, Seoul 08826, Korea & Center for Nanoparticle Research, Institute for Basic Science (IBS), Seoul 151-742, Korea

Chemical synthesis allows for realizing semiconductor nanocrystals with high perfection. Varying composition, shape and size facilitates tailoring the bandgap and targeted doping can be used to add additional functionality. E. g., transition metals embedded into the host matrix of CdSe nanocrystals may act as efficient luminescence centers. Thus, the question arises how such luminescence centers can be activated and what finally controls the emission of doped nanocrystals. Here, we discuss how intra- and interparticle energy transfer processes affect the luminescence of size- and shape engineered colloidal CdSe nanocrystals doped with Cu and Mn, respectively.

The photoluminescence of quasi-2D CdSe nanoplatelets (NPLs) shows unique signatures like up to three distinct emission lines below 100 K. There seems to be consensus that besides neutral excitons negative trions contribute to the emission, but their prominent role with regard to spherical nanocrystals is rather puzzling. We demonstrate that interparticle Förster resonant energy transfer in stacks of CdSe NPLs combined with hole trap states in specific NPLs within the stack triggers trion formation, while single NPL spectra are dominated by neutral excitonic emission. This interpretation is verified by implementing Cu dopants into the lattice as intentional hole traps that enforce trion formation [1].

In the ultimate limit of magic-sized $(CdSe)_{13}$ cluster (MSC) doping with individual transition metal ions like Mn [2] could be achieved. Probing the characteristic Mn^{2+} luminescence allows the differentiation between the intraparticle energy transfer from excitonic fine structure states to Mn^{2+} monomers and to Mn^{2+}-Mn^{2+} dimers, respectively [3]. Whereas the internal $^4T_1$ - $^6A_1$ Mn^{2+} emission dominates the emission pattern in Mn-doped MSC, undoped $(CdSe)_{13}$ clusters reveal a broad luminescence band below the bandgap. This can be attributed to exciton-driven polaron formation enforced by surface traps, a hypothesis that is supported by a comparison of the experimental data with DFT calculations [4].

[1] Riesner, M., Shabani, F., Zeylmans van Emmichoven, L., Klein, J., Delikanli, S., Fainblat, R., Demir, H.V., Bacher, G., ACS Nano **18** (2024) 24523; doi.org/10.1021/acsnano.4c08776
[2] Yang, J., Fainblat, R., Kwon, S.G., Muckel, F., Yu, J.H., Terlinden, H., Kim, B.H., Iavarone, D., Choi, M.K., Kim, I.Y., Park, I., Hong, H.-K., Lee, J., Son, J.S., Lee, Z., Kang, K., Hwang, S.J., Bacher, G., Hyeon, T., J. Am. Chem. Soc. **137** (2015) 12776; doi.org/10.1021/jacs.5b07888
[3] Bieniek, J., Baek, W., Lorenz, S., Muckel, F., Fainblat, R., Hyeon, T., Bacher G., Nano Research **17** (2024) 10669; doi.org/10.1007/s12274-024-7108-1
[4] Bieniek, J., Steenbock, T., Baek, W., Drescher, E., von Toperczer, F., Hyeon, T., Bester, G., Bacher, G., Small Structures **6** (2025) e202500392; doi.org/10.1002/sstr.202500392

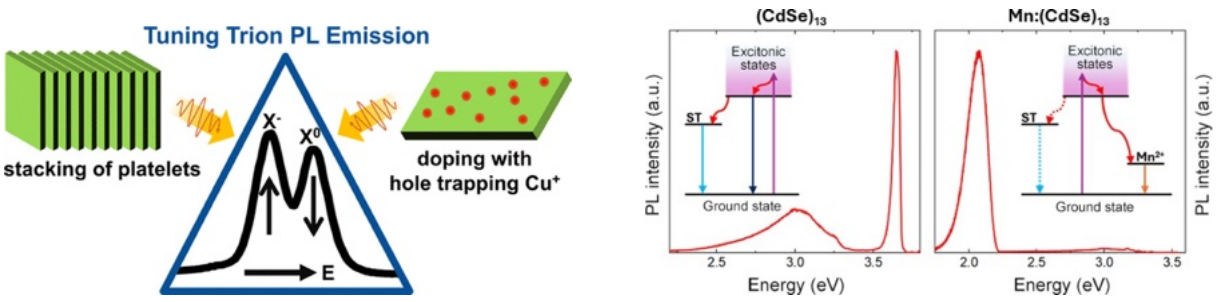

Fig. 1: Left: Concept of controlling the trion to neutral exciton ratio in CdSe NPL via interparticle energy transfer between NPL and intraparticle energy transfer to Cu-dopants, respectively [1]. Right: Intraparticle energy transfer from excitonic states to surface traps and to Mn dopants, respectively [3].

Notes

Indium oxide nanocrystals as excited state electron acceptors

Wayne L. Gladfelter, Mik Patel, and David A. Blank

Department of Chemistry, University of Minnesota, Minneapolis, MN 55455, USA

Light initiated excited state electron transfer (ESET) from organic chromophores to metal oxides is central to the functioning of dye-sensitized solar cells and related devices. Titanium and zinc oxides have been extensively studied for these applications, however, interest in carrier multiplication via triplet fission has focused on metal oxides with lower conduction band energies which can accept electrons from low energy triplet states. Among the binary metal oxides, indium oxide, In_2O_3, has one of the lower energy conduction bands. This initial study quantifies the binding and ESET rates of (E)-2-cyano-3-[5-[4(diethylamino)phenyl]thiophen-2-yl]-2-propenoic acid, **1**, and (E)-2-cyano-3-[5-[4(diethylamino)phenyl]furan-2-yl]-2-propenoic acid, **2**, to well-defined nanocrystals (NCs) of In_2O_3 and compares the results to previous studies using ZnO NCs.[1]

Size-uniform colloidal oleate-capped In_2O_3 NCs were synthesized using a continuous growth method. [2] The In_2O_3 NCs were found to quench the emission of **1** and **2** upon binding. Emission quenching of **1** and **2** was used to quantify oleate substitution on the NCs through a competitive exchange Langmuir model [3] resulting in exchange equilibrium constant values of 22 ± 7 and 8 ± 1 and maximum dye surface coverage values of 400 ± 20 and 420 ± 10 dyes/NC, respectively. Based on the cross-sectional area of the dyes, the dyes were found to occupy approximately half the surface area of the NC. The emission quenching was confirmed to result from electron transfer using spectroelectrochemisty and ultrafast pump-probe spectroscopy. Electron transfer time constants for **1** and **2** of 1.79 ± 0.05 ps and 1.28 ± 0.07 ps, respectively, were obtained, which were ~8 times shorter than those to ZnO NCs. The faster rates were attributed to differences in electronic coupling and density of NC acceptor states in In_2O_3.

[1] Swedin, R., Badgurjar, D., Healy, A., Harkins, R., Oehrlein, A., Greenlund, L., Alshebber, M., Ripp, N., Anderson, N. T., Honzay, B. R., Pappenfus, T. M., Janzen, D. E., Blank, D. A., Gladfelter, W. L., *J. Phys. Chem. C*, 124, **2020,** 15565, doi/10.1021/acs.jpcc.0c03828.
[2] Jansons, A. W., Hutchison, J. E., *ACS Nano*, 10, **2016**, 6942, doi/10.1021/acsnano.6b02796.
[3] Greytak, A. B., Abiodun, S. L., Burrell, J. M., Cook, E. N., Jayaweera, N. P., Moinul Islam, M., Shaker, A. E., *Chem. Commun.*, 58, **2022**, 13037, doi.org/10.1039/D2CC05012A.

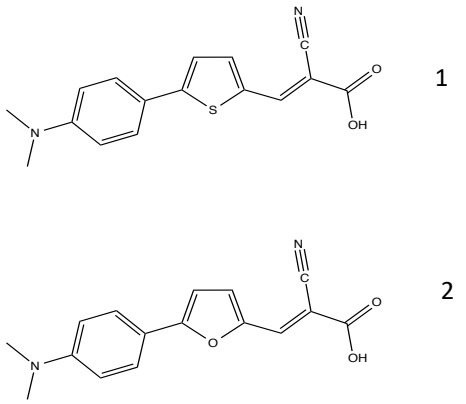

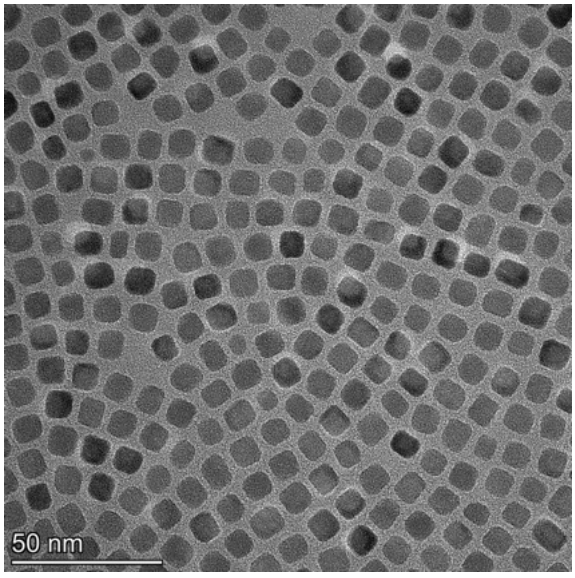

Fig. 1: Dye structures **1** and **2** and TEM of oleate-capped In_2O_3 nanocrystals

Notes

First-principles modeling of optoelectronic properties and strain engineering in II-VI chalcogenide alloys and core-shell nanostructures

André Schleife and Erick Hernandez

Department of Materials Science and Engineering, University of Illinois at Urbana-Champaign, 61801, Urbana, Illinois, USA

After introducing the first-principles simulation framework used in our work, this talk focuses on the theoretical characterization of zincblende HgxCd1−xS and HgxCd1−xSe ternary alloys, materials critical for near- to far-infrared photodetector and photoemission applications. Addressing the challenge that modeling alloyed systems requires maintaining configurational randomness beyond simple periodic images, this study employs a cluster expansion approach combined with the generalized quasi-chemical approximation (GQCA) to predict properties at thermodynamic equilibrium. Using density functional theory (DFT) with the HSE06 hybrid functional and including spin-orbit coupling (SOC), the electronic structure and optical response are calculated for the binary endpoints and intermediate compositions.
The inclusion of SOC is found to be essential, revealing a Dresselhaus-Rashba splitting in HgS and HgSe and converting them from zero-gap semimetals to materials with small indirect band gaps. For the alloys, the study predicts dielectric functions and band gap energies at 300 K, identifying a nonlinear polynomial relationship between composition and the energies of the E1 and E2 spectral peaks. Consistent with the principles of modeling alloys, which necessitate accounting for strain and atomic geometry, the GQCA method allows for the determination of bowing parameters, offering a robust reference for optical metrology of these less-explored chalcogenides.

Next, this study addresses challenges of modeling finite nanostructures, specifically CdSe/CdS core-shell nanoplatelets. Surface relaxation is critical, and the role of strain profiles resulting from atomic geometry cannot be omitted. Consequently, this study utilizes explicit slab models to simulate epitaxial growth and confinement effects, rather than relying on bulk approximations. The research utilizes DFT to relax lattice parameters and atomic coordinates, allowing for the precise calculation of strain projections.

The results indicate that shell growth induces a significant red-shift in the band gap energy, a phenomenon driven primarily by changes in the valence band dispersion rather than conduction band shifts. The modeling reveals a complex strain landscape where the core undergoes compression while the shell experiences tension, confirming that alloy and heterostructure composition strongly influences the strain profile. This explicit simulation of slab models effectively bridges the gap between bulk quantum well models and the experimental reality of colloidal growth, providing a detailed understanding of how strain anisotropy and quantum confinement interact to tune the optoelectronic properties.

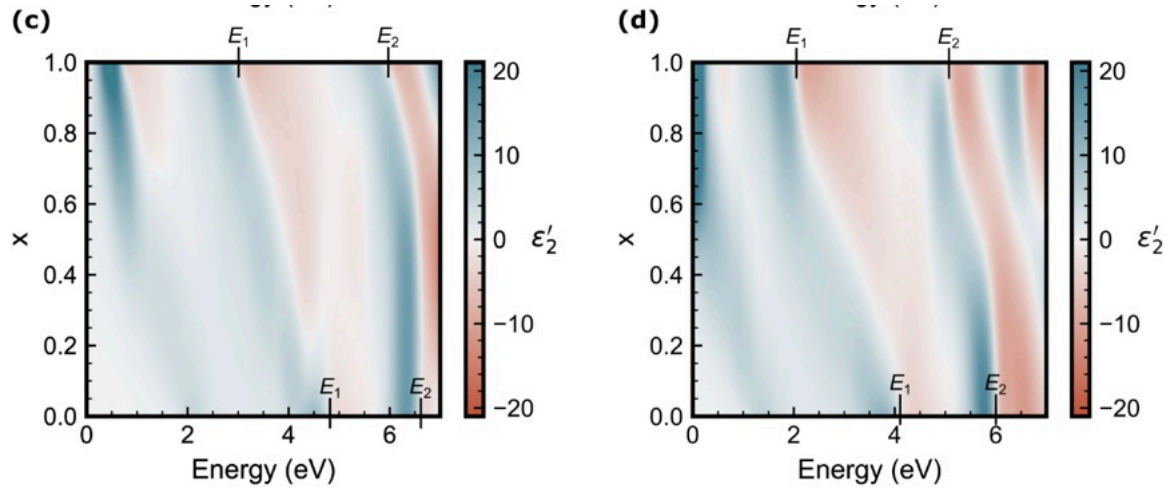

Fig. 1: First derivatives of the imaginary part of the dielectric function for $Hg_xCd_{1-x}S$ and $Hg_xCd_{1-x}Se$.

Notes

Rationalizing quantum-dot behavior in flame-formed carbon nanoparticles: from accurate excitation energies to stacking effects

Luna Pratali Maffei[1], A. Nobili[2], N. Kateris[3], A. S. Jayaraman[2], M. Tommasini[1], and H. Wang[2]

1 Department of Chemistry, Materials and Chemical Engineering, Politecnico di Milano, Milan, 20133, Italy
2 Department of Mechanical Engineering, Stanford University, Stanford, California 94305, United States
3 Department of Engineering, University of Cambridge, Cambridge, CB2 1PZ, United Kingdom

Accurate prediction of the electronic and optical properties of polycyclic aromatic hydrocarbons (PAHs) is critical to understanding the gas-phase formation of nano-carbon materials. In fact, the band gap of a CNP is likely governed by its PAH constituent with the smallest energy gap [2]. Likely constituents of small CNPs (d_p = 2–4 nm) exhibiting quantum-dot behavior are aromatic islands with up to 20 aromatic rings, with the main PAH families of interest including peri-condensed molecular PAHs and resonance-stabilized π-radicals [3]. In literature, HOMO-LUMO gaps derived from DFT calculations are widely adopted as estimates for the optical band gaps of PAHs and CNPs. However, the accuracy of this method has not been assessed for open-shell species. In this work, we report accurate CASPT2 calculations for excitation energies E_{0n} and oscillator strengths f_{0n} for transitions from the ground state to low-lying excited states (n = 1-3) for PAH molecules, cation radicals, and π-radicals. The computed E_{0n} values show good agreement with available absorption and photoionization measurements. TD-DFT calculations, also performed for comparison, reproduce the general trend observed in multireference calculations, with errors below 0.3 eV. Finally, the HOMO-LUMO gaps obtained from DFT calculations agree with the CASPT2 excitation energies for molecules (left panel of Fig. 1). However, predictions for open-shell species do not exhibit similar quantitative agreement. In fact, HOMO-LUMO gaps in π-radicals and cations generally reproduce the trends of E_{02}, but show errors of 1–1.5 eV for E_{01} (example: middle panel in Fig. 1). Hence, corrections are necessary when employing DFT to investigate energy gaps in open-shell species. This work provides insight into the species that are likely to be found in flame-formed CNPs: delocalized radicals with embedded 5-membered rings (group B in the figure) are compatible with measured optical band gaps (1.5 eV) of small CNPs collected in flames [1]. Exploring the impact of π-radical stacking by DFT (right panel in Fig. 1), we observe that the formation of a C-C bond systematically increases HOMO-LUMO gaps of π-radical dimers. On the other hand, non-covalently bonded dimers have lower (if relying on DFT) or similar (considering corrections from CASPT2 calculations) gaps compared to the π-radical monomers. The present findings will contribute to improve estimates of PAH and CNP optical properties and their characterization.

[1] C. Liu, A. V. Singh, C. Saggese et al., *PNAS.* **116**, 26 (2019) 2692-12697.
[2] N. Kateris, A. S. Jayaraman, H. Wang, *Proc. Comb. Inst.* **39**, 1 (2023) 1069–1077.
[3] J. W. Martin, M. Salamanca, M. Kraft, *Prog. En. Comb. Sci.* **88** (2022) 100956.

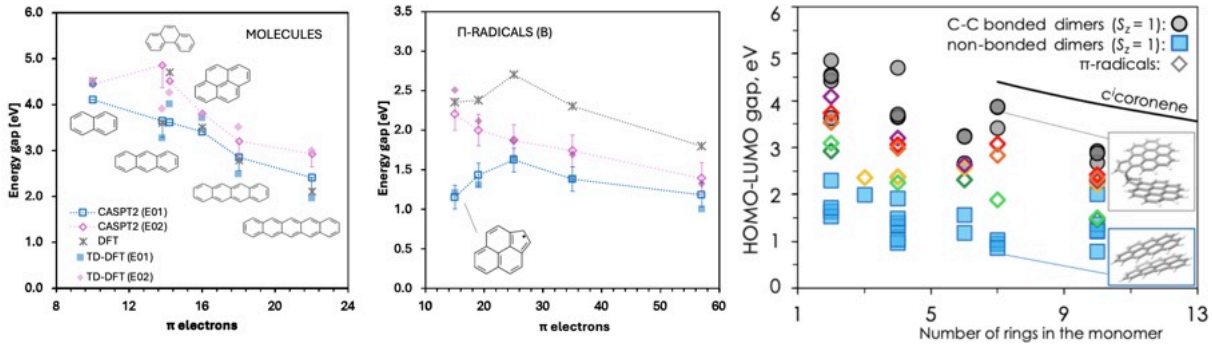

Fig. 1: Left, middle: CASPT2, TD-DFT and DFT results for energy gaps (first and second vertical excitation energies) for closed-shell PAHs and a relevant class of π-radical PAHs, respectively. Right: investigation of stacking effects for different classes of π-radical PAH monomers (empty symbols) upon formation of non-bonded (blue) or σ-bonded (black) dimers on DFT HOMO-LUMO gaps.

Notes

2D semiconductors: defects, interfaces, and new opportunities

Marika Schleberger, Stephan Sleziona, Leon Daniel, and Jennifer Schmeink

University of Duisburg-Essen, Faculty of Physics and CENIDE, 47057 Duisburg, Germany

In modern electronics, the active material can be only a few atoms thick, so defects and interfaces play a decisive role in device performance. For example, in silicon field-effect transistors (FETs), the carrier mobility typically degrades as channel dimensions shrink, largely because surface/interface scattering and electrically active interface states, often associated with dangling bonds at the Si/oxide interface, become increasingly important.

In the search for alternative channel materials, two-dimensional (2D) materials have attracted growing interest. Owing to their van der Waals bonding, they can be fabricated with an atomically uniform thickness – often down to a single monolayer (for TMDCs: a three-atomic-plane X–M–X sheet) – and, ideally, with no out-of-plane dangling bonds and minimal strain.

Transition metal dichalcogenides (TMDCs) such as MoS_2 and WS_2 are particularly attractive because they become direct-gap semiconductors in the monolayer limit, with band gaps in (or near) the visible range, enabling a wide range of optoelectronic applications. However, the active channel materials' properties are strongly controlled by defects, see e.g. ref. [1]. Depending on the application, defects can be either beneficial or detrimental—posing a challenge, but also offering an opportunity for defect engineering [2,3] and for designing optimized or even entirely new device concepts [4].

More recently, *Janus* TMDC monolayers (e.g., MoSSe, with different chalcogens on the two sides, see Fig. 1 [5]) and *Janus alloys* [6] have emerged as a compelling extension: the broken out-of-plane symmetry introduces an intrinsic dipole and can substantially modify band alignment, screening, and defect physics—providing additional knobs to tailor electronic and optoelectronic functionality.

[1] R. Zheng, L. Daniel, D. Sutarma, Ch. Viernes, Y. Ding, T. Fabunmi, G. Bacher, M. Heuken, H. Kalish, A. Vescan, P. Kratzer, M. Schleberger, G. Sciaini, Chem. Sci. **17** (2026) 1176; https://doi.org/10.1039/D5SC07343J

[2] S. Sleziona, A. Pelella, E. Faella, O. Kharsah, L. Skopinski, A. Maas, Y. Liebsch, J. Schmeink, A. Di Bartolomeo, M. Schleberger, Nanoscale Adv., **5** (2023) 6958; https://doi.org/10.1039/D3NA00543G

[3] L. Daniel, D. Sutarma, O. Kharsah, C. Lintz, P. Kratzer, M. Schleberger, ACS Nanoscience Au (2025),

[4] S. M. Hus, R. Ge, P.-A. Chen, L. Liang, G.E. Donnelly, W. Ko, F. Huang, M.-H. Chiang, A.-P. Li, D. Akinwande, Nat. Nanotechnol., **16** (2021) 58; https://doi.org/10.1038/s41565-020-00789-w

[5] J. Schmeink, V. Musytschuk, E. Pollmann, St. Sleziona, A. Maas, P. Kratzer, M. Schleberger, Nanoscale, **15** (2023) 10834; https://doi.org/10.1039/D3NR01978K

[6] J. Schmeink, J. Osterfeld, O. Kharsah, St. Sleziona, M. Schleberger, npj 2D Mat. Appl., **8** (2024) 67; https://doi.org/10.1038/s41699-024-00504-6

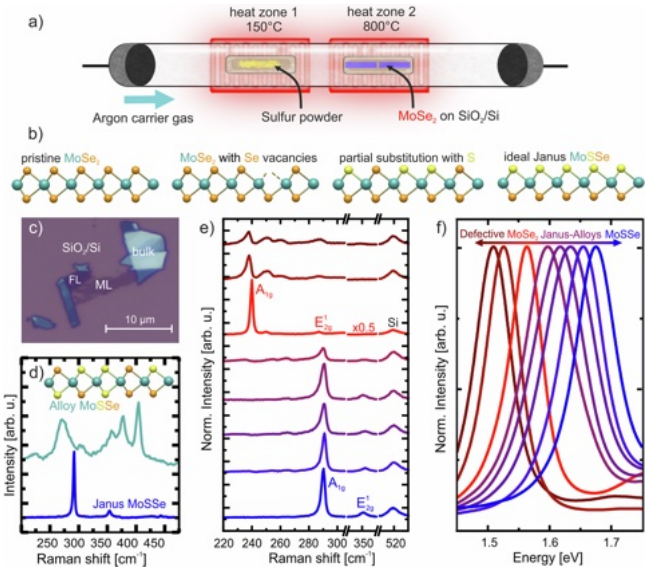

Fig. 1: Janus TMDCs [5]: a) Fabrication by thermal post-processing of exfoliated $MoSe_2$ monolayers (optical microscopy image in c). b) Depending on the process parameters, the full range of configurations can be realized—from pristine $MoSe_2$ to defect-rich $MoSe_2$, through MoSSe alloys, and ultimately to ideally ordered Janus MoSSe. d) – f) Raman and PL spectroscopy show distinct differences between monolayer Janus, Janus alloys and bulk alloy; PL emission can be tuned via the stoichiometry.

Notes

Optical monitoring of substrate doping in MOCVD grown MoS_2 monolayers

Tilmar Kümmell[1], Henrik Myja[1], Dennis Schlotthauer[1], Pawan Kumar[2], Benjamin Groven[2], Steven Brems[2], Henry Medina Silva[2], Pierre Morin[2], and Gerd Bacher[1]

1 Werkstoffe der Elektrotechnik, University Duisburg-Essen, Bismarckstr. 81, 47057 Duisburg, Germany
2 IMEC, Kapeldreef 75, 3001 Leuven, Belgium

Transition metal dichalcogenides (TMDCs) like molybdenum disulfide (MoS_2) are emerging ultrathin materials for various fields of application, including electronics, sensors, memory devices and optoelectronics. Metal organic chemical vapor deposition (MOCVD) is the most promising approach to synthesize wafer scale TMDC monolayers (ML), a key requirement for implementing TDMCs in future scalable devices. One main challenge hereby is the control of the doping level in the TMDCs, which usually is a complex interplay between doping via defect formation and remote doping either from the substrate or from the environment. Photoluminescence (PL) spectroscopy has been proven to be a sensitive tool for elucidating the impact of defects or substrate on TMDC doping [1, 2], but it still remains highly challenging to disentangle the individual contributions to the TMDC doping level.

We employ temperature- and ambient-controlled PL spectroscopy to reveal doping mechanisms in MoS_2 grown on sapphire and afterwards transferred to device-grade Si/SiO_2 substrates. 1.2 ML of MoS_2 was deposited on 2-inch c-plane sapphire by MOCVD with $Mo(CO)_6$ and H_2S precursors using an industry-standard 200 mm CVD reactor [3]. We compare polycrystalline and single-crystalline ML of MoS_2 [3, 4], realized by different growth times.

Experiments at low temperature (5.5 K) reveal a substantially different contribution of defect emission for single-crystalline and polycrystalline MoS_2 on sapphire. The single-crystalline MoS_2 exhibits a very weak defect PL and clear near band edge emission, while the polycrystalline MoS_2 emission is controlled by an intense defect contribution. We attribute these findings to a different sapphire morphology as a consequence of the different growth time. Thus, in the case of the single-crystalline MoS_2 we assume n-doping of the TMDC by the substrate [1], saturating the defect emission at low temperature. In contrast, doping is reduced in polycrystalline MoS_2, making the defect clearly visible. This approach is backed up by room temperature PL measurements: The signal of the single-crystalline MoS_2 is dominated by low-intensity charged exciton emission, indicating n-doping, while the polycrystalline sample shows an intense neutral exciton emission (Fig. 1, left). After transferring both ML to Si/SiO_2, their difference in PL signatures largely disappears (Fig.1, right). Obviously, the impact of the substrate on the PL is by far more important than the influence of the grain boundaries.

[1] Y. Zhu et al., The Journal of Physical Chemistry C **17**, 8294 (2025)
[2] K. T. Munson et al. The Journal of Physical Chemistry Letters, **15** (2024) 7850
[3] Y. Shi et al. ACS Nano, **15** (2021) 9482
[4] I. Kandybka et al. ACS Nano, **18** (2024) 3173

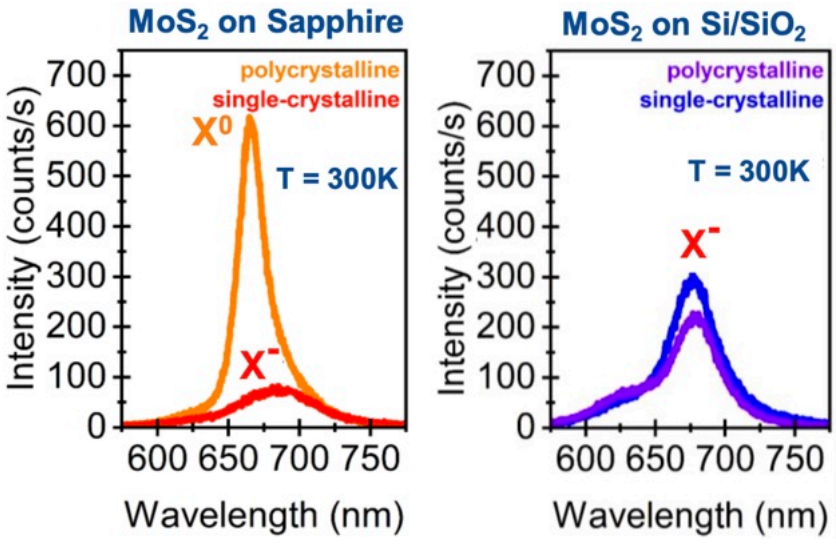

Fig. 1: Room temperature PL spectra of polycrystalline and single-crystalline MoS_2 monolayers on sapphire (left) and on Si/SiO_2 (right), indicating different substrate doping.

Notes

Grain-boundary states enable charge separation and narrowband photoresponse in 2D perovskites

Franziska Münzer, Markus Winterer, Tamara Czerny, Florian Von Toperczer, Julius Konietzka, Qian Shen, Jochen Konieczny, and Martin A. Schroer

Werkstoffe der Elektrotechnik & CENIDE, University Duisburg-Essen, 47057 Duisburg, Germany

Two-dimensional (2D) Ruddlesden–Popper perovskites consist of metal halide layers separated by organic spacer cations, resulting in pronounced quantum and dielectric confinement and consequently large exciton binding energies. Despite this, efficient charge carrier separation has been reported, yet the microscopic mechanisms enabling this process remains incompletely understood. Here, we present a comprehensive experimental study that elucidates exciton dissociation and charge separation pathways in 2D perovskite thin films.

Using a custom-built experimental platform, we perform simultaneous, spatially resolved photocurrent and photoluminescence (PL) mapping, enabling direct correlation of local optical emission and charge transport. The combined maps reveal strongly enhanced photocurrent generation at grain boundaries, accompanied by a redshifted and anisotropic PL emission. These observations indicate the presence of specific intragap states localized at grain boundaries that promote exciton dissociation. By comparing photocurrent maps recorded under inverted bias conditions, these states are identified as electron traps within the band gap, providing a driving force for charge separation. [1]

Beyond mechanistic insights, we demonstrate a direct functional implication of these findings by exploiting the spectrally narrow excitonic transition in 2D Ruddlesden–Popper perovskites to realize intrinsically narrowband photodetectors. Devices based on interdigitated electrodes exhibit a pronounced narrowband photoresponse corresponding to the excitonic absorption, with response times of approximately 150 µs, external quantum efficiencies up to 9%, and responsivities reaching 38 mA/W. [2]

Overall, this work establishes a direct link between nanoscale defect physics and optoelectronic functionality in 2D perovskites, providing design guidelines for photovoltaic and narrowband photodetection applications.

[1] Czerny, T., Von Toperczer, F., Konietzka, J., Münzer, F., ACS Energy Letters 2025, 10 (11), 5965–5971; https://doi.org/10.1021/acsenergylett.5c03352

[2] Czerny, T., Shen, Q., Konieczny, J., Schroer, M. A., Winterer, M., Münzer, F., J. Phys. Chem. Lett. 2023, 14 (20), 4850–4857; https://doi.org/10.1021/acs.jpclett.3c00710

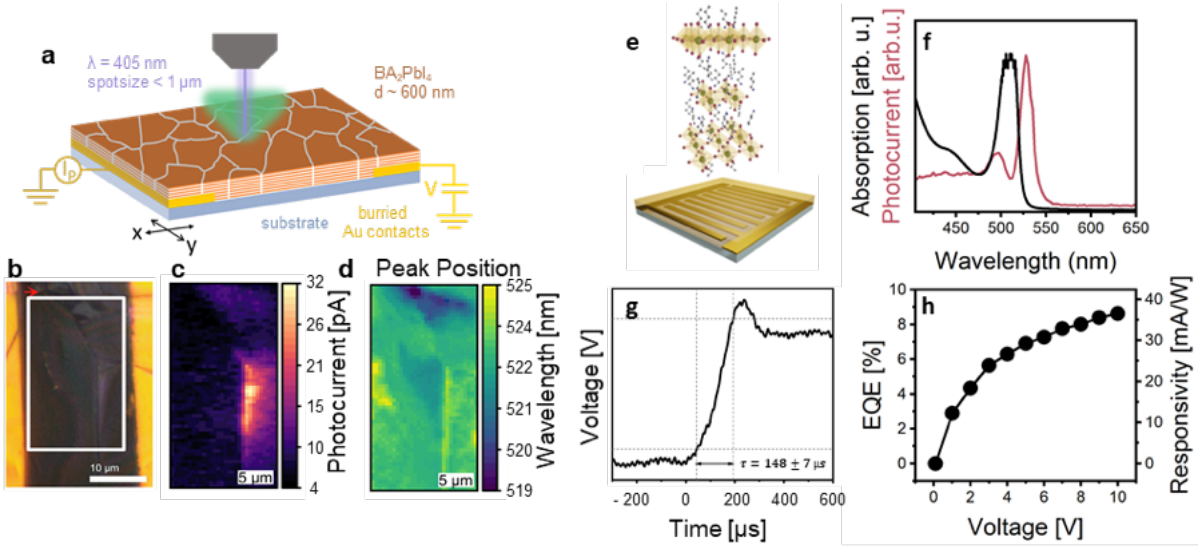

Fig. 1: a) Schematic of the experimental setup. b) Optical microscopy image of the device area and the corresponding c) photocurrent and d) PL map. e) Scheme of the device. f) Comparison of absorption and photocurrent spectrum. g) Temporal response of the device. h) Voltage-dependent EQE

Notes

Synchrotron X-ray nano-analysis & imaging

Julie Villanova[1], Sandra Benter[1], Valentina Bonino[1], Didier Bouvard[2], Jaime Dolado[1], Cyril Guilloud[1], Madeleine Han[1], Benjamin Holliger[1], Pierre Lhuissier[2], Rémi Tucoulou[1], Victor Vanpeene[3,1], and Aatreya Venkatesh[2,1]

1 ESRF – The European Synchrotron, Grenoble, France
2 Univ. Grenoble Alpes, CNRS, Grenoble INP, SIMAP, F-38000 Grenoble, France
3 Univ. Grenoble Alpes, CEA, CNRS, Grenoble INP, IRIG, SyMMES, 38000 Grenoble, France

Synchrotron X-ray nano-analysis and imaging encompass several X-ray techniques that provide high spatial resolution information on the composition, crystalline and electronic structure, and internal microstructure of small objects. The beamline ID16B at the ESRF [1] is dedicated to hard X-ray 2D and 3D nano-analysis and nano-imaging, offering a versatile combination of methods, including X-ray fluorescence (XRF), X-ray absorption spectroscopy (XAS), X-ray excited optical luminescence (XEOL and TR-XEOL), X-ray diffraction (XRD), and 3D/4D X-ray nano-imaging (nano-CT). With the advent of fourth-generation synchrotron sources, these capabilities have been extended to 4D imaging, enabling the study of dynamic processes and in situ experiments.

This presentation will highlight the beamline's capabilities in terms of spatial resolution and practical applications. The techniques can be employed individually or combined to enable 2D and 3D multimodal analyses of nanostructures, trace element distributions, phase behavior, microstructures, and functional properties in a non-destructive manner. Selected scientific examples on nano-materials will illustrate these capabilities. In the final part of the presentation, special emphasis will be placed on recent studies of the 3D analysis of ceramic powder sintering [2-4].

[1] Martinez-Criado G., J Synchrotron Radiat, **23** (2016) 344 ; doi.org/10.1107/S1600577515019839.
[2] Venkatesh A., J. Eur. Ceram. Soc., **43** (2023) 2553 ; doi.org/10.1016/j.jeurceramsoc.2022.12.065.
[3] Venkatesh A., Ceram. Int., **50** (2024) 4715 ; doi.org/10.1016/j.ceramint.2023.11.216.
[4] Venkatesh A., J. Eur. Ceram. Soc., **44** (2024) 7236 ; doi.org/10.1016/j.jeurceramsoc.2024.05.027.

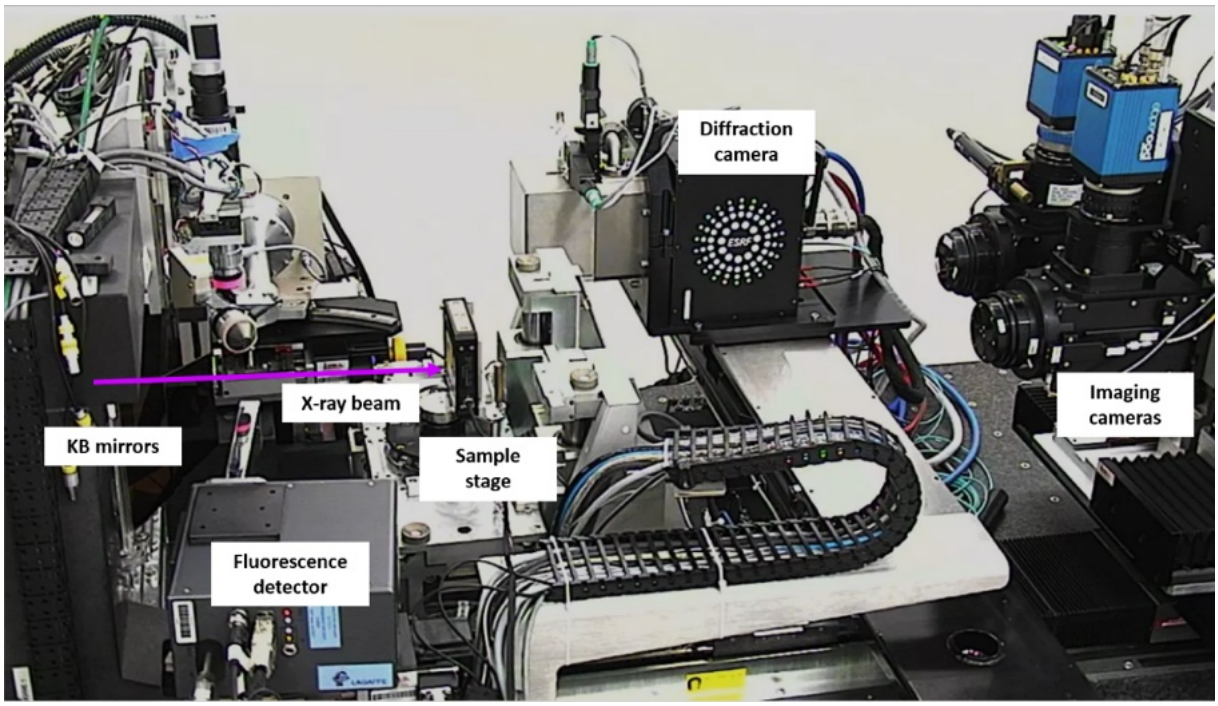

Fig. 1: Picture of the experimental setup at ID16B. It illustrates the combination of the different techniques used for simultaneous 2D or 3D spatially resolved measurements of microstructure, composition, crystalline and electronic structure of a material.

Notes

Observing the evolution of nanocrystals by *in situ* and *operando* X-ray diffraction during Chemical Vapor Synthesis

Shradha R. Joshi, Martin A. Schroer, and Markus Winterer

Nanoparticle Process Technology, Universität Duisburg-Essen, 47057 Duisburg, Germany

Chemical vapor synthesis (CVS) is a gas-phase production technique yielding nanoparticles (NPs) of high purity, crystallinity, narrow size distribution, and low degree of hard agglomeration [1]. The design of NPs with desired properties is enabled by the control of the CVS process parameters and demands a fundamental understanding of CVS. Conventional *ex situ* characterization of CVS-generated NPs can suffer from artifacts during particle collection, such as preferred orientations, aggregation, oxidation or aging of nanocrystals. This can be circumvented by studying the formation processes *in situ* [2] and *operando* probing, i.e., *where* and *while* the particles form.

Here, we report results on X-ray diffraction (also known as Wide Angle X-ray scattering or WAXS) of tin oxide NPs probed *in situ* during CVS to observe the evolving crystal structure as the particles form and grow [3]. Special focus is placed on the variation of the *T(t)* profile of the CVS reactor and observing its influence on the crystal structure of NPs, *in situ*. Additionally, simulations of the CVS process with the program cvssinmc [4] are performed with process parameters analogous to the *in situ* experiments to interpret the associated formation mechanism and compare the resulting particle characteristics. *In situ* experimental results supported by simulations indicate a dynamic evolution of the NP structure.

A major challenge of *in situ* measurements during CVS is the weak diffraction signal of the very dilute sample system of NPs in the gas phase. However, a combination of a synchrotron radiation source - where these experiments are performed, sensitive X-ray detectors, and a dedicated experimental set-up [5] designed especially for *in situ* X-ray studies enables direct observation by high-quality diffraction signals.

[1] Winterer, M., *Nanocrystalline Ceramics: Synthesis and Structure*, Berlin: Springer 2002
[2] Joshi, S. R., Schroer, M. A., Winterer, M., Chem. Mater. **37** (2025) 5710; doi.org/10.1021/acs.chemmater.5c00848
[3] Joshi, S. R., Schroer, M. A., Winterer, M., Chem. Mater. (2026) doi.org/10.1021/acs.chemmater.6c00089
[4] Winterer, M., Chem. Eng. Sci. **186** (2018) 135; doi.org/ 10.1016/j.ces.2018.04.005
[5] Schroer, M. A., Levish, A., Yildizlar, Y., Stepponat, M., Winterer. M., Rev. Sci. Instr. **93** (2022) 113706; doi.org/10.1063/5.0122461

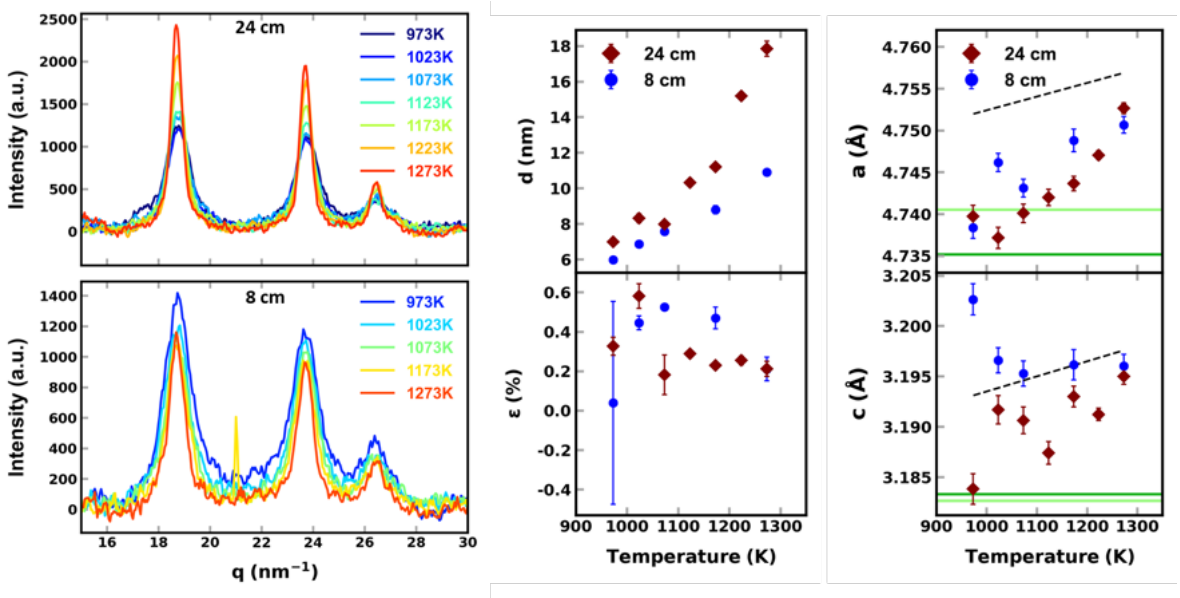

Fig 1. Results of *in situ* X-ray diffraction of tin oxide nanoparticles probed during CVS for long (24 cm) and short (8 cm) heating zones with corresponding trends of crystal structure parameters plotted as a function of temperature obtained from Rietveld refinement.

Notes

Deciphering the agglomerate structure of nanoparticle dispersions for medical applications by X-ray scattering

Martin A. Schroer[1,2], Maria Paola Demichelis[3,4], Patrizia Sommi[4,5], and Umberto Anselmi-Tamburini[3,4]

1 Nanoparticle Process Technology (NPPT), Faculty of Engineering, University of Duisburg-Essen, 47057 Duisburg, Germany
2 Center for Nanointegration Duisburg-Essen (CENIDE), University of Duisburg-Essen, 47057 Duisburg, Germany
3 Department of Chemistry, University of Pavia, 27100 Pavia, Italy
4 Unit of Pavia, National Institute of Nuclear Physics, INFN, 27100 Pavia, Italy
5 Department of Molecular Medicine, University of Pavia, 27100 Pavia, Italy

Medical applications of nanoparticles require the stable dispersion in compatible media to enable their correct functionality. Agglomeration of nanoparticles can limit their theranostic performance, affect the cell uptake and result in unwanted, potentially toxic, reactions. Therefore, it is important to characterize in advance the agglomeration behavior within the relevant medical media and model cell systems. Especially the local clustering of particles is important to prevent such unwanted reactions by optimized sample treatment.

The structural characterization of agglomerates in dispersion is commonly performed by dynamic light scattering (DLS) measurements, which yield information limited to size and size distribution, as structure and morphology are beyond the resolution of light scattering techniques.

This limitation can be overcome when combining it with small angle X-ray scattering (SAXS). SAXS allows the study of structure and interactions of nanoparticles in dispersions over a length scale range from Angstroms to several 100 nanometers and yields structural information under physiologically relevant conditions, enabling multiscale analysis.

One frequent challenge is the interpretation of SAXS profiles resulting from agglomerates, in particular, when interested in the local clustering of nanoparticles into larger structures. For this, we started employing an *ab initio* modeling-based approach, originally developed for SAXS from biological macromolecules, which enables the determination of agglomerate morphology. Complementing SAXS modeling with data from asymmetric flow field flow fractionation (AF4)-DLS and powder X-ray diffraction data, the agglomerate assembly can be deciphered for nanoparticles in different media.

This approach is demonstrated for two types of nanoparticle systems, developed for medical applications: Antioxidant ultra-small ceria (CeO_2) particles [1] and boron-rich assemblies composed of boron carbide B_4C particles and iron oxide Fe_3O_4 particles [2].

This presentation will further show recent results from X-ray scattering experiments to study agglomeration of nanoparticles directly within HeLa cells.

[1] Sommi, P., Vitali, A., Coniglio, S., Callegari, D., Barbieri, S., Casu, A., Falqui, A., Vigano, L., Vigani, B., Ferrari, F., Anselmi-Tamburini, U., ACS Nano, **15** (2021) 15803; 10.1021/acsnano.1c03151
[2] Demichelis, M.P., Portu, A.M., Gadan, M.A., Vitali, A., Forlingieri, V., Bortolussi, S., Postuma, I., Falqui, A., Vezzoli, E., Milanese, C., Sommi, P., Anselmi-Tamburini, U., Appl. Nano, **5** (2024) 33; 10.3390/applnano5020004

Acknowledgements: We thank Markus Winterer for his continuous support.

Notes

Silicon-based nanostructured calibration standards for traceable scanning probe microscopy

D. Banaś[1], D. Czułek[2], K. Domański[4], **Janusz Fidelus[1,2]**, M. Goliszek-Chabros[3], P. Jagodziński[1,2], P. Janus[4], A. Kubala-Kukuś[1], M. Kucharska[4], U. Maciołek[3], A. Nowicka[3], P. Prokaryn[4], A. Sierakowski[4], K. Skrzypiec[3], W. Sofińska-Chmiel[3], I. Stabrawa[1], and K. Szary[1]

1 Institute of Physics, Jan Kochanowski University, PL-25-406 Kielce, Poland
2 Central Office of Measures, PL-00-139 Warszawa, Poland
3 Maria Curie-Skłodowska University, PL-20-031 Lublin, Poland
4 Łukasiewicz-Institute of Microelectronics and Photonics, PL-02-668 Warszawa, Poland

Accurate SPM measurements necessitate robust and dimensionally stable calibration standards. In this contribution, we present the design, fabrication, and metrological evaluation of silicon-based nanostructured calibration patterns intended for routine use in atomic force microscopy (AFM) and scanning tunneling microscopy (STM).

The calibration standards were fabricated using a combination of silicon micromachining, electron-beam lithography, and projection photolithography, resulting in highly periodic structures with half-pitch dimensions of 0.25 µm and 1 µm over areas of 3 mm × 3 mm. Such large-area periodicity facilitates navigation and localization, particularly in STM, which in turn supports reliable lateral scale calibration. Metrological characterization was carried out using independently calibrated AFM and STM systems, bolstered by certified reference standards. Image analysis was comprehensive, as it accounted for scanner nonlinearity, probe convolution effects, and data processing artifacts.

Preliminary results indicate excellent dimensional uniformity, reproducibility, and long-term stability of the fabricated patterns, affirming their suitability as traceable SPM calibration standards. Ongoing interlaboratory comparisons will further quantify measurement uncertainty and promote the dissemination of traceable nanoscale length standards within the nanoscale physical measurements community.

The project is co-financed from the state budget by the Minister of Education and Science under the Polish Metrology II program (registration number PM-II/SP/0044/2024/02).

Notes

The diffusivity of tiny nanoparticles in the gas phase

Sotiris E. Pratsinis

Department of Mechanical & Process Engineering, ETH Zurich, CH 8092 Zurich, Switzerland

Tiny nanoparticles (TNPs) are particles of equivalent diameter smaller than 5 nm. In the literature, they have been referred to loosely as clusters, quantum dots, ultrafine particles or just nanoparticles. The TNPs have many potential applications and play a pivotal role in the atmosphere. There TNPs grow into larger aerosol particles that reduce visibility and adversely affect air quality, human health and climate. For example, formation and growth of atmospheric TNPs from 1.7 to 3.0 nm leads to a 50% increase in the predicted concentrations of cloud condensation nuclei, having important implications on climate. At the same time, nanostructured particles (or nanoparticles, NPs) are used routinely as dispersions, films and in devices (i.e., gas sensors, smartphones, etc). These NPs are made *en masse* by gas- or liquid-phase processes. Between the two, gas-phase (aerosol) processes are most effective in manufacturing diverse compositions and morphologies of NPs to tons/hour (carbon blacks, fumed oxides etc.) for a wide spectrum of products and applications.

Three years ago I presented here in Venice during our MiFuN conference a new kinetic theory of gases that accounted for, in addition to the well-known repulsive forces between air molecules, also for attractive forced between air molecules and their diatomic shape, for the first time [1]. This was in stark contrast to the classic kinetic theory of gases that treats them as perfect spheres undergoing solely elastic (ballistic) collisions [2]. As it was shown then this new theory showed that air molecules undergo largely inelastic head on, grazing and orbiting-like collisions (Fig. 1) besides the elastic head on collisions quoted in all physics textbooks. A recalculation of the mean free path (MFP) in air accounting for such forces showed that the MFP is about half that cited in all textbooks of gas dynamics [1]. Such a discovery affects all gas-phase transport processes at the nanoscale. For example, the diffusivity of TNPs in air is up *to an order of magnitude lower* than that listed in textbooks as the particle or cluster size approaches the size of the surrounding gas molecules, in excellent agreement with experimental measurements [3]. As time permits, I will explain these fascinating results through the fundamentals of diffusion in gases revealing a new understanding of nanoscale transport in gases.

[1] Tsalikis DG, Mavrantzas VG, Pratsinis SE, *Physics of Fluids,* **35**, 097131 (2023). DOI: 10.1063/5.0166283
[2] Maxwell JCMA, *The London, Edinburgh, Dublin Philos. Mag. J. Sci.*, **19** (1860) 19, DOI: 10.1080/14786446008642818
[3] Karadima KS, Tsalikis DG, Mavrantzas VG, Pratsinis SE, *J. Phys. Chem. A,* **129** (2025) 5127, DOI: 10.1021/acs.jpca.5c00407

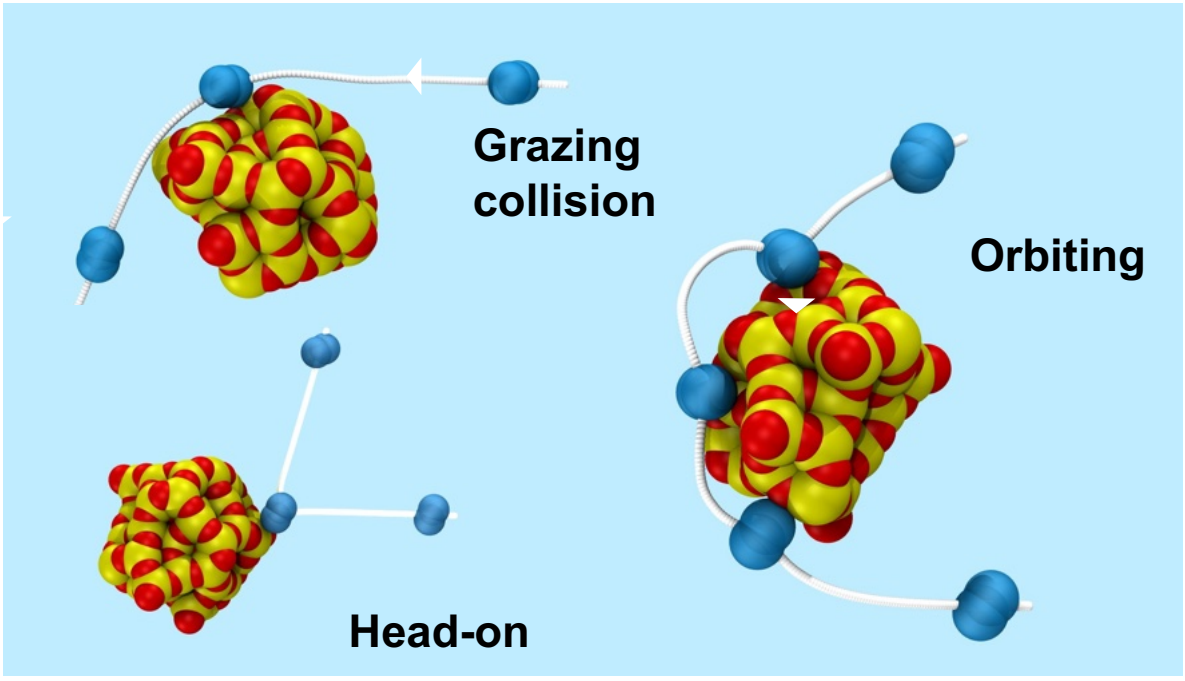

Fig. 1: Collision types of N_2 molecules (blue dumbbells) with a 1.5 nm SiO_2 nanoparticle consisting of yellow and red silicon and oxygen atoms

Notes

Mass spectrometric Investigation of gas phase reactions of aluminium acetylacetonate with water and oxygen

Burak Atakan[1], Sebastian Grimm[1], Andras Bodi[2], Patrick Hemberger[2], Nina Gaiser[3], Thomas Bierkandt[3], and Ilyas Adaköy[1]

1 Thermodynamics (EMPI) and Cenide, University of Duisburg-Essen, D-47057 Duisburg, Germany
2 Laboratory for Synchrotron Radiation and Femtochemistry, Paul Scherrer Institute, CH-5232 Villigen-PSI, Switzerland
3 Institute of Combustion Technology, German Aerospace Center (DLR), Pfaffenwaldring 38-40, Stuttgart, 70569, Germany

The controlled synthesis of aluminium oxide (Al_2O_3) thin films by metal–organic chemical vapour deposition (MOCVD) or in vapour phase nanoparticle synthesis critically depends on the decomposition behaviour of its metal–organic precursors in the gas phase. Aluminium acetylacetonate ($Al(acac)_3$) is one of the most commonly employed precursors owing to its low toxicity, moderate sublimation temperature and thermal stability. Despite its wide use, the mechanistic understanding of its gas-phase chemistry in the presence of reactive carrier gases such as water vapour and oxygen remains incomplete. In this work, we present a systematic mass spectrometric study of the gas-phase decomposition of $Al(acac)_3$ under CVD-relevant residence times and pressures, using vacuum ultraviolet (VUV) synchrotron radiation coupled with double imaging photoelectron photoion coincidence spectroscopy (i²PEPICO). Temperature-dependent spectra were recorded for both humid (Ar + H_2O) and oxygen-containing carrier gas environments, allowing for the identification of stable products, transient intermediates and decomposition pathways.

In the presence of water vapour, the precursor decomposes at lower temperatures faster than under inert conditions, consistent with a water-mediated proton transfer that bypasses the energetically unfavourable intramolecular four-membered transition state. This pathway accelerates hydrolysis and enhances the release of acetylacetone and acetone, while suppressing the formation of characteristic intermediates such as $Al(C_5H_7O_2)_2H$. Furthermore, systematic variation of residence time and water concentration revealed that higher water fractions significantly increase precursor conversion, corroborating earlier MOCVD studies reporting enhanced film growth rates and ligand-free Al_2O_3 layers. In contrast, oxygen exhibited a marked-ly different behaviour: instead of mirroring the inert atmosphere at lower temperatures, the $Al(acac)_3$ signal remained nearly constant over a broad range, which is most plausibly explained by reversible reaction channels that regenerate the precursor. Only above 700 K did the oxygen begin to promote alternative gas-phase decomposition pathways, particularly the formation of ketene and other oxygenated hydrocarbons. These results provide new mechanistic insight into the interplay between precursor chemistry and reactive gas atmospheres in MOCVD and highlight the distinct, non-equivalent roles of water vapour and oxygen in influencing deposition kinetics and film properties.

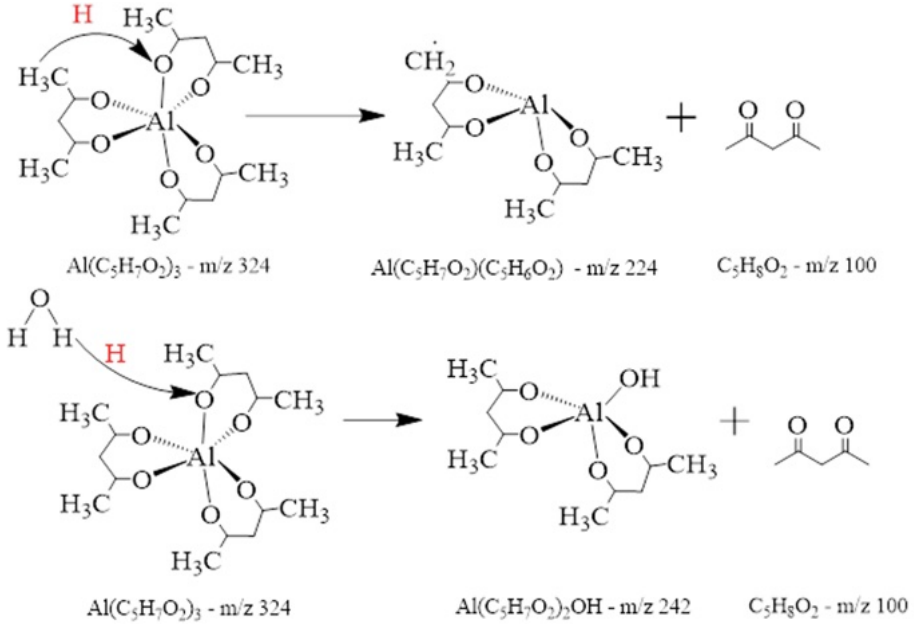

Fig. 1: Proposed first decomposition steps with water vapor and without water vapor. The proton transfer is indicated in red with the black arrow.

Notes

Pulsed precursor flow in chemical vapor synthesis and deposition of oxides as nanocrystals and epitaxial thin films

Felipe F. Morgado, Chuxiang Qi, and Markus Winterer

Nanoparticle Process Technology and CENIDE, University of Duisburg-Essen, 47057 Duisburg, Germany

Titanium dioxide (TiO_2) nanoparticles or films are employed in versatile applications such as photocatalysis or chemical sensing. Precise control over synthesis and thorough structural characterization are essential to tailor corresponding physicochemical. Here, we present a pulsed precursor flow approach in chemical vapor synthesis (CVS) and deposition (CVD) to generate TiO_2 in form of nanoparticles with finely tuned structural properties and epitaxial thin films. The pulsed delivery of precursors allows modulation of growth kinetics and control over nucleation, enabling the formation uniformly sized nanoparticles and highly oriented films.

CO_2 laser light is pulsed using a shutter and the solid metal organic precursor is delivered to the CVS / CVD reactor in form of precursor pulses. Detailed structural analysis is conducted using X-ray powder diffraction and high-resolution X-ray diffraction (HRXRD) combined with detailed data analysis. HRXRD methods such as rocking curve, reciprocal space mapping (RSM), X-ray reflectivity (XRR), and ω–2θ scans provide key insights into lattice parameters, strain states, film thickness, and crystallographic orientation relative to the substrate. In addition, transmission electron microscopy (TEM) is utilized to analyse the nanoscale morphology, crystallinity, and size distribution of TiO_2 nanoparticles and films, confirming uniform particle distribution (PSD) and epitaxial relationships to the $LaAlO_3$ substrates.

We observe predominantly TiO_2 in form of the anatase phase with nanoparticles exhibiting narrow PSD, and epitaxial (00l) thin films with a thickness below 200 nm. The narrow rocking curve widths (FWHM < 0.2°) and pronounced interference fringes observed in the XRD data indicate high crystal quality films. The RSM measurement indicates a strained film in relation to the $LaAlO_3$ substrate. Complementary, the nanoparticle size and their PSD width decreases with decreasing laser pulse length, as observed in the TEM images.

The pulsed precursor flow and multi-technique characterization approach enables a comprehensive understanding of the mechanisms governing nanoparticle formation and epitaxial growth. Such insights facilitate the correlation of structural features with functional properties and contribute to the progress of synthesis of nanoparticles and thin oxide films. The methodology is promising for in-depth study of other nanomaterials with critical applications in catalysis, sensors, and energy devices.

Notes

Formation of coral-like nanostructures on nickel surfaces via remote nitrogen plasma treatment

Nicolas Wöhrl[1], Christina Meinert[1], Karla Sieker[1], Timo Wagner[1], Christian Marcks[3], Vineetha Vinayakumar[2], Doris Segets[2], and Axel Lorke[1]

1 Faculty of Physics and CENIDE, University of Duisburg-Essen, 47057 Duisburg, Germany
2 Institute for Energy and Materials Processes, University of Duisburg-Essen, 47057 Duisburg, Germany
3 Electrochemical Reaction Engineering, RWTH Aachen University, 52074 Aachen, Germany

Nickel electrodes are the industrial standard for electrolyzers due to their low cost and abundance. We demonstrate that a microwave-induced remote nitrogen plasma treatment is an effective approach to tailor the surface morphology and chemistry of these nickel electrodes. The plasma treatment induces the formation of coral-like nanostructures (Fig. 1) and results in measurable surface nitridation, which together lead to increased surface roughness and improved wettability [1]. In this contribution, we demonstrate how these modified surface properties translate into enhanced functional performance, specifically improved electrochemical activity in alkaline water electrolysis systems. This correlation is demonstrated by contact angle measurements and 3D optical profilometry to quantify the surface modification, as well as by electrochemical characterization to assess the resulting catalytic behavior.

In addition, remote nitrogen plasma treatment can be effectively integrated as a post-processing step for coated electrodes, especially for Ni–Co–O nanoparticle electrocatalyst layers. Plasma post-treatment improves coating adhesion and mechanical stability while simultaneously removing organic contaminants and binder residues originating from the coating process, which would otherwise block active sites and reduce electrolysis efficiency. This results in enhanced wettability, improved redox reversibility, and more reproducible electrochemical performance [2].

Overall, our results establish the remote nitrogen plasma treatment as a versatile and scalable surface engineering strategy for nickel and nickel-based substrate surfaces in alkaline water electrolysis systems.

[1] Wagner, T. et al., Surf. Coat. Technol., **505** (2025) 132056; https://doi.org/10.1016/j.surfcoat.2025.132056
[2] Vinayakumar, V. et al., *Chem. Eng. J.* **523** (2025) 167169; https://doi.org/10.1016/j.cej.2025.167169

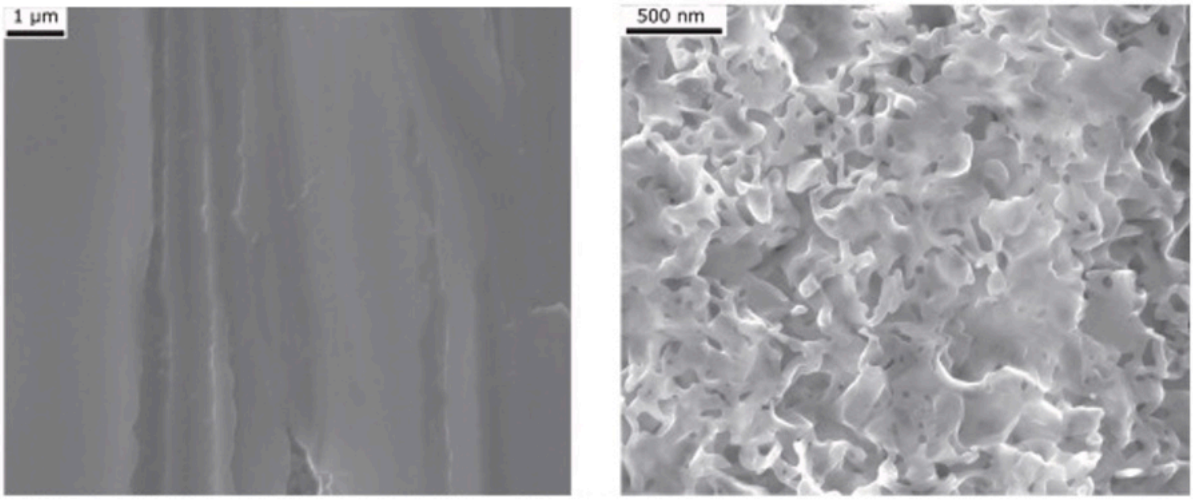

Fig. 1: SEM images of the untreated nickel surface (left) reveal a characteristic relief pattern originating from the rolling process during manufacturing, while the surface remains otherwise flat and smooth. In contrast, the same nickel surface after 10 min of nitrogen plasma treatment (right) exhibits a pronounced morphological transformation, characterized by the formation of a porous surface structure.

Notes

Plasma-induced optically active defects in the van-der-Waals material hBN (hexagonal boron nitride)

Felix Schaumburg, David Plitt, Timo Wagner, Nicolas Wöhrl, Martin Geller, Günther Prinz, and **Axel Lorke**

Faculty of Physics and CENIDE, University Duisburg-Essen, 47057 Duisburg, Germany

Hexagonal boron nitride (hBN) has become an important material for van der Waals heterostructures, in particular for cladding layers. However, hBN can also serve as a host material for optically active defects. These defects can exhibit single photon emission, even at room temperature, which makes them attractive for novel applications in quantum information technologies and sensing applications.

Plasma treatment has shown to be a promising method to induce spatially and spectrally tailored photon emitters in hBN. Different plasma species and procedures have been reported in the literature. Therefore, a systematic study on how specific gas species affect the optical properties of the created defects is desirable.

Here, we present a direct comparison of defect emission in exfoliated hBN after plasma treatment, using three distinct chemical species: Argon, which will only interact physically with hBN; nitrogen as a constituent of the hBN host material; and oxygen as a foreign and chemically reactive element.

Hexagonal boron nitride was exfoliated on Si/SiO_2 substrates [1]. Before any plasma treatment, the hBN flakes were mapped by scanning micro-photoluminescence (μ-PL) spectroscopy, to ensure that only plasma-induced defects were investigated. For the same reason, no annealing step was performed.

The samples were then exposed for 90s to the different gas species in a custom-built remote microwave plasma reactor (600W, 5mbar). Using scanning PL again, we identified newly created emission spots of high brightness and narrow line width as most promising candidates for single color center formation.

For Ar plasma exposure and 532nm laser excitation, we find luminescence in a narrow region around 600nm. No PL is observed for longer (633nm) or shorter (405nm) excitation wavelengths. This indicates that Ar exposure mainly induces a single kind of optically active defect, which results in efficient luminescence when the excitation and the emission are separated by approximately one LO phonon energy. [2]

Nitrogen and oxygen plasma, on the other hand, result in a much broader spread of emission energies, ranging from ≈420nm via ≈580nm up to ≈720nm (for 405, 532 and 633nm excitation, respectively). This shows that N and O treatment leads to a variety of defects, while Ar plasma induces more uniform, specific color centers. [2]

Extended plasma exposure was used to create more uniform and overall more intense luminescence. Samples that were plasma irradiated for 300s exhibited broad and bright emission. We found the best results for exposure to the chemically inert Ar species, while the ablation caused by the O plasma led to a saturation of the emitter density.

[1] Schaumburg, F., Sleziona, S., Zöllner, M., Dergianlis, V., Schleberger, M., Geller, M., Lorke, A., Prinz, G.; Appl. Phys. Lett. **123**, (2023) 073101; doi.org/10.1063/5.0159365

[2] Schaumburg, F., Plitt, D., Wagner, T., Wöhrl, N., Geller, M., Prinz, G., and Lorke, A.; Appl. Phys. Lett. **126**, (2025) 043103; doi.org/10.1063/5.0253028

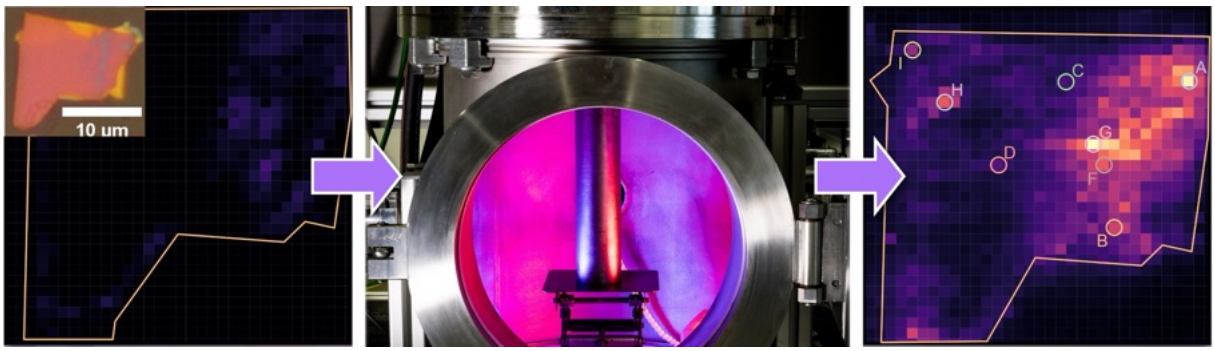

Fig. 1: (left) Optical microscope image of an hBN flake (inset) and its photoluminescence map, which shows only minute photoemission. Orange lines indicate the outline of the flake. After remote plasma exposure (center), individual emitters can be seen in the luminescence map (right).

Notes

Aerosol CNT synthesis at scale – what is needed for kilo-tonne to megatonne production?

Adam Boies[1,2], Jack Peden[1], Shahzad Hussein[1], Michael Glerum[1], and Joe Stallard[1]

1 Department of Engineering, University of Cambridge, Cambridge, CB21PZ, UK
2 Department of Mechanical Engineering, Stanford University, Stanford, CA, 94305, USA

Aerosol-based processes are emerging as a transformative pathway for the co-production of carbon nanotubes (CNTs) and turquoise hydrogen via catalytically induced methane pyrolysis. While this area has grown rapidly, there remains an unsettled optimization of critical products, production scales, and the underlying physical and chemical understanding of these processes. This talk highlights recent advances and outstanding challenges in scaling aerosol-phase synthesis to meet industrial needs for both high-performance nanocarbon-based macromaterials. The rapidly expanding lithium-ion battery market is a key driver of CNT demand, while the scale of hydrogen production implies that far more solid carbon will be generated than is currently utilized, raising critical questions about the societal value of engineered nanocarbons.

Large-scale reactor design must balance control of aerosol-phase nucleation with the engineering of bulk material properties. In the last 24 months, CNT-based materials have achieved ultimate tensile strengths that surpass those of the world's best carbon fibers and have made exciting advances in electrical conductivity, now surpassing copper and aluminium on a mass basis. However, fundamental uncertainties remain in aerosol kinetics, particularly aerogel formation and its role in multi-scale morphology. Improved understanding and control of catalyst nucleation, growth, and utilization are equally central, yet CNT catalysts currently achieve only ~0.1% efficiency.

To translate these advances into impact, rapid scaling is underway in the US and Asia. Emerging in-situ optical diagnostics and aerosol measurement tools offer unprecedented insights into reaction zones, enabling the design of densified reactors and opening pathways to new one-dimensional materials with extraordinary properties.

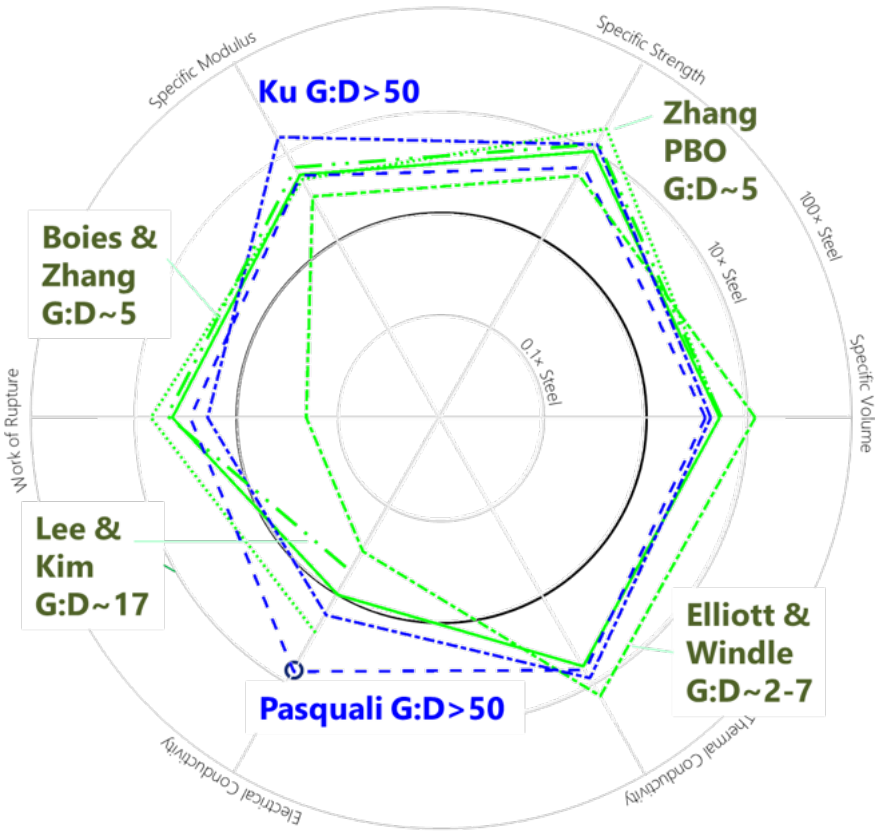

Fig. 1: Recent high performance CNT-fiber characteristics as produced from floating catalyst aerosol chemical vapor deposition processes.

Notes

Formation of free-standing graphene in microwave plasma synthesis

Paolo Fortugno, Ornel Padilla, Hartmut Wiggers, and **Christof Schulz**

EMPI, Institute for Energy and Materials Processes – Reactive Fluids, and CENIDE, Center for Nanointegration Duisburg Essen, University of Duisburg-Essen, 47048 Duisburg, Germany

Microwave plasma synthesis is emerging as a scalable, continuous, and substrate-free method for producing high-quality few-layer graphene (FLG). Advancing this technique requires a deeper understanding of the conditions that lead to the formation of either FLG or soot-like structures. Understanding the reaction conditions that delimit FLG and soot formation will be essential for designing production strategies for FLG with target properties in high yield. This research investigates the precursor decomposition pathways, nucleation processes, and growth dynamics of carbonaceous species at high temperature, aiming to identify the operating conditions that favor FLG formation [1].

In the plasma process, FLG synthesis begins with the thermal decomposition of hydrocarbon precursors in the high-temperature plasma zone (>2000 K). Prior studies indicate that FLG synthesis follows a radical-driven growth process via the hydrogen-abstraction/carbon-addition (HACA) pathway [2]. This mechanism is kinetically favored in regions of high radical density and temperature, supporting the extension of planar aromatic structures. The formation of soot-like particles, on the other hand, is driven by the rapid formation and interaction of polycyclic aromatic hydrocarbons (PAH) that dominate under conditions of high supersaturation and thus high precursor concentration and lower temperature. Therefore, careful control of precursor flow, energy density, time–temperature profile and plasma parameters is essential to favor graphene nucleation and suppress the formation of soot-like particles.

To further understand the temperature dependence of the graphene-FLG bifurcation, shock-tube experiments have been conducted to investigate the transition from soot to graphene formation at the high-temperature limit of particle formation after hydrocarbon pyrolysis. The results confirm that FLG forms under select reaction conditions, reinforcing the hypothesis that specific temperature profiles, precursors, and concentrations are critical to prefer graphene growth over soot formation.

The morphology variation starting from flat single-atom layers to increasingly crumpled and multilayer structures is investigated by thermophoretic sampling from the plasma flow and provides insight into an “origami” process [3] where – after an initial nucleation and growth of single-layer graphene in the gas phase – a sequence of folding and crumpling dominates the final morphology of the product.

[1] Fortugno, P., Lopez Camara, C.-F., Hagen, F., Wiggers, H., Schulz, C., Appl. Energ. Combust. Sci. **15** (2023) 100180; doi.org/10.1016/j.jaecs.2023.100180.
[2] Fortugno, P., Musikhin, S., Shi, X., Wang, H., Wiggers, H., Schulz, C., Carbon **186** (2021) 560-573; doi.org/10.1016/j.carbon.2021.10.047.
[3] López-Cámara, C-F., Fortugno, P., Heidelmann, M., Wiggers, H., Schulz, C., Carbon **218** (2024) 118732; doi.org/10.1016/j.carbon.2023.118732.

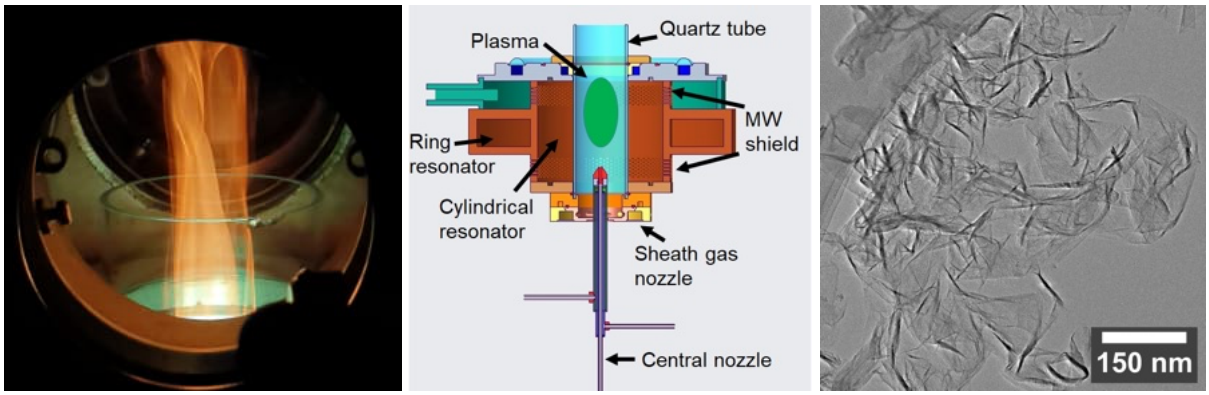

Fig. 1: Microwave plasma synthesis of free-standing few-layer graphene from hydrocarbon precursors.

Notes

Spray-flame synthesis of inorganic multi-element oxides

Hartmut Wiggers[1,2], Steven Angel[1], Leon Müller[1], and Mohammed-Ali Sheikh[1]

1 Institute for Energy and Materials Processes – Reactive Fluids (EMPI-RF), University of Duisburg-Essen, 47057 Duisburg, Germany
2 Center for Nanointegration Duisburg-Essen (CENIDE), University of Duisburg-Essen, 47057 Duisburg, Germany

Some of the most important nanoscale raw materials for industry – pyrogenic silica, titanium dioxide, and carbon black – have been produced on a 1000-ton scale for many decades using continuous gas phase processes. These materials are characterized by very high purity, and the manufacturing process benefits from the fact that, apart from gas phase species, only a few process-related material flows need to be handled. In contrast, more complex multi-element oxides are often produced in batch processes using liquid or solid phase synthesis.

This presentation aims to show that multi-element nanomaterials can also be produced excellently using gas phase-based processes. Based on a detailed understanding of the particle formation processes in spray flames, the successful synthesis of nanoscale catalyst materials is demonstrated using the example of spinels and perovskites from spray flame synthesis which is based on the atomization and combustion of metal salt solutions. In addition to the selection of suitable solvent combinations, which ideally enable complete transfer of the metal oxide precursors dissolved in them to the gas phase, it is shown that the chemical composition of the precursors also influences the size and morphology of the nanoparticles produced. This could be attributed, among other things, to the complexation of the metal ions in the precursor solution as well as to chemical reactions in the solution. One focus of our work is the production of catalysts for the oxidation of hydrocarbons and the oxygen evolution reaction (OER), the most important step in electrochemical water splitting. Examples will be used to demonstrate the successful production of high-performance catalyst materials from spray flame synthesis.
Based on our findings on the targeted production of multi-element oxides, we have succeeded in applying this concept to the production of entropy-stabilized oxides, with the presentation highlighting the limits of entropy stabilization for certain materials.

[1] Angel, S., Braun, M., Alkan, B., Landers, J., Salamon, S., Wende, H., Andronescu, C., Schulz, C., Wiggers, H., J. Phys. Chem. A, **127** (2023) 2564; doi.org/10.1021/acs.jpca.2c06601
[2] Sheikh, M.-A., Angel, S., Schleich, S., Müller, L., Ternieden, J., Schulz, C., Wiggers, H., under review

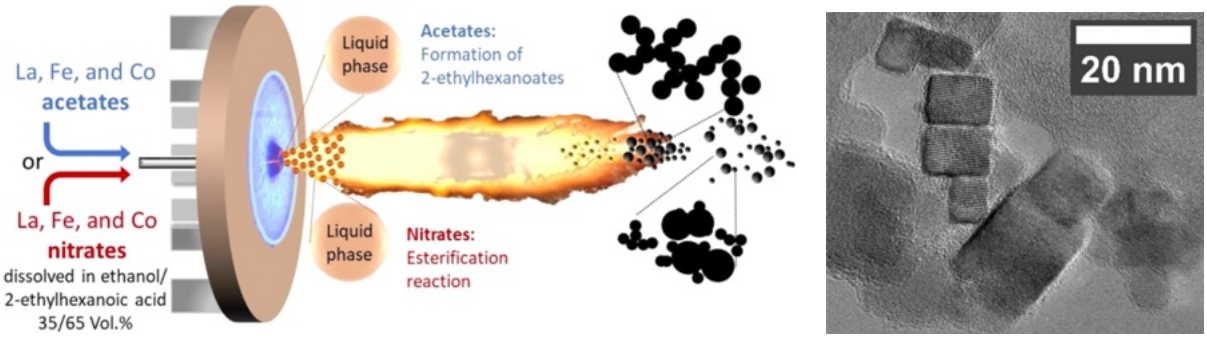

Fig. 1: Schematic diagram of nanoparticle synthesis in a spray flame reactor (left) [1] and TEM image of cubic high-entropy oxide nanoparticles from spray flame synthesis (right) [2].

Notes

Real-time control of nanoparticle synthesis by spark ablation

F. Einar Kruis[1], Jonah V. Weidemann[1], Danijel Čuturić[2], and Steven X. Ding[2]

1 Institute of Technology for Nanostructures, University of Duisburg-Essen, 47057 Duisburg, Germany
2 Institute for Automatic Control and Complex Systems, University of Duisburg-Essen, 47057 Duisburg, Germany

Spark ablation is an electrical discharge method for producing nanoparticles of a large variety of materials from solid electrodes through evaporation and subsequent homogeneous nucleation, followed by aggregate formation via coagulation and sintering with constituent particles measuring only a few nm. However, the changing plasma conditions as a result of electrode erosion causes the process to be inherently dynamic. A real-time control system solves these issues by guiding the process using meaningful particle properties. The key performance indicators (KPIs), defining the output properties of spark ablation synthesis, are measured on-line. The main challenge here is to measure the primary particle size and the product loading of the gas, for which no commercial aerosol instrumentation is available. This would provide insights into the mesostructure of the particles (i.e., primary particle diameter d_p and number of primary particles per aggregate n_p) and the total mass production rate $\dot{m}$.

KPI calculation is possible on the basis of simultaneous measurement of the distributions of particle mobility (Partector 2 Pro, Naneos, Windisch, Switzerland) and aerodynamic size (ELPI+, Dekati Ltd., Kangasala, Finland) from rapid, parallel measurements with a time-resolution of 1 s. Control variables are the electrode distance d_{el}, charging current I and gas flowrate $\dot{V}$. The control system employs machine learning methods trained on this input and output data to ensure accuracy, adaptability, and robustness.

A key component of that system is a bivariate, monodisperse particle formation model predicting the evolution of aggregate surface area and volume, incorporating their fractal-like nature. A hybrid spark model additionally allows to gain insights regarding hidden variables that define the synthesis conditions, i.e., the evaporation rate yielding the initial monomer concentration c_0 and the temperature-time profile, which in first approximation is defined through a constant effective temperature T_{eff} and residence time τ_{res}. Fig. 1 show that the monitoring system is able to track the KPIs closely when instantaneously changing the control variables

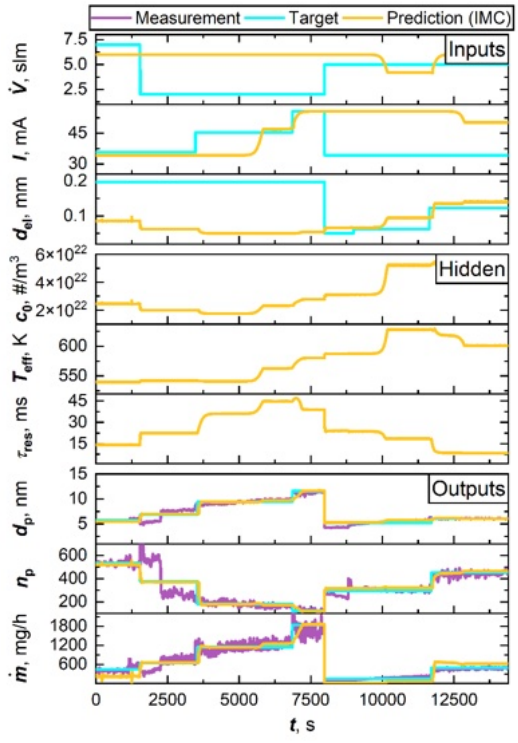

Figure 1: Monitoring the Key Performance Indicators (outputs) by controlling the spark synthesis variables (inputs) driven by rapid online measurements of electric mobility and aerodynamic diameter

Notes

Grain boundary development between nanoparticles: evidence from rapid sintering of alumina

Richard I. Todd and David Zonghao Guo

Department of Materials, University of Oxford, Oxford OX1 3PH, UK

When nanoparticles of different orientation are in contact at high temperature, a grain boundary forms between them. Atomistic modelling gives interesting indications of pathways for structure development in developing grain boundaries but their properties in the earliest stages of formation are difficult to access experimentally owing to their transient nature.

This presentation investigates diffusion rates in grain boundaries forming between nanoparticles using rapid sintering of alumina nanopowder compacts. These are heated with widely differing heating rates (0.1-100 K/s). The slowest heating rates correspond to conventional heating in a furnace and the fastest are achieved using „ultra-fast high temperature sintering“ (UHS), in which low thermal mass carbon felts surrounding thin samples are heated electrically. Detailed analysis of the densification rates shows that sintering at a given temperature and relative density is accelerated by rapid heating. This is partly accounted for by microstructural refinement but if this is allowed for, an increase in grain boundary diffusion coefficient at a given temperature and relative density by up to a factor of 20 under the fastest heating rate compared with the slowest is implied.

This indirect result is directly investigated by further experiments in which particles of Cr_2O_3 are added to the alumina compacts as a chemically compatible diffusion tracer. The diffusion of the Cr_2O_3 into the surrounding alumina during sintering is investigated using EDX line scans. The results demonstrate an acceleration of diffusion in UHS correlating well with the sintering results. The acceleration only occurs during the early stages of sintering, however; eventually the diffusion rates in UHS and conventional sintering become the same.

On the basis of atomistic modelling results from the literature, it is suggested that the initial acceleration of diffusion is a consequence of the formation of non-equilibrium, probably metastable grain boundaries with high energy, less compact structures and correspondingly high diffusion coefficients in the early stages of sintering. These can be reconciled with recent ideas concerning grain boundary „complexions“ – different 2-dimensional grain boundary structures with character and behaviour similar in many ways to 3-dimensional crystal phases.

There are obvious practical applications of this work in rapid and energy efficient processing of materials, which was the original motivation of the research.

Notes

A time-resolved exploration of resonant laser sintering

Jeldrik Schulte, Martin A. Schroer, and Markus Winterer

Nanoparticle Process Technology, Faculty of Engineering and CENIDE, University of Duisburg-Essen, 47057 Duisburg, Germany

Resonant laser sintering (RLS) of complex oxides from nanoscaled metal oxide precursors is a unique and innovative approach for the production of novel materials via solid-state reactions [1]. In contrast to conventional sintering of powders in crucibles using furnaces, for which the entire sample material is heated for a long time, laser-sintering allows for localized and fast (of the order of milliseconds) sintering. Using nanoscaled particles results in a reduction of the sintering temperature compared to bulk materials due to the particle size-effect. In combination with 2D printing or other thin film deposition techniques, RLS enables the production of structured layers and therefore holds potential for use in printable (opto-) electronics [2] or sensors, even on flexible polymeric substrates. Especially by using photons with energies larger than the band gap of the (unsintered) green body, fast and resonant heating is achieved with rather low total power laser systems [1]. These extreme heating rates as well as the subsequent cooling rates strongly affect the sintering process. Thus, the resulting (micro-) structures can be adjusted by the variation of laser power density and exposure time. However, producing functional nanomaterials from nanoparticles requires precise control and thorough understanding of the process temperature-time profile.

We will present an *operando* study using combined wide- and small- angle X-ray scattering with high-speed thermography during RLS to uncover time-resolved structural transitions on the nanoscale.

[1] Mackert, V., Gebauer, J.S., Notthoff, C., Winterer M, Appl. Surf.Sci. **457**, (2018) 1174; doi**:** 10.1016/j.apsusc.2018.06.304
[2] Garlapati, K., Gebauer, J S., Dehm, S., Bruns, M., Winterer, M., Hahn, H. and Dasgupta S, Adv. Electron. Mater. **3** (2017), 6.; doi: 10.1002/aelm.201600476

Notes

Flash effect on reduction- and oxidation-fronts propagating through TiO_2

Dietrich E. Wolf[1], Vikaskumar Mishra[2], and Devinder Yadav[2]

1 Faculty of Physics and CENIDE, University of Duisburg-Essen, 47057 Duisburg, Germany
2 Department of Metallurgical and Materials Engineering, IIT Patna, 801106 Patna, India

Densely sintered TiO_2 samples that are exposed to a constant current, while being in the state of flash, may show a remarkable phenomenon under certain conditions [1]: Starting from the cathode the ion conductor TiO_2 progressively changes into sub-oxide TiO_{2-x} with high electronic conductivity. The sub-oxide does not sustain the flash anymore; the glow retreats towards the anode. Surprisingly, after a stochastic waiting time the glow reappears at the cathode and spreads towards the anode. The sub-oxide converts back into the pristine phase TiO_2, in which the flash ignites again. Subsequently the pristine phase gets reduced again, and so forth. The reduction front propagates distinctly slower than the oxidation front (Fig. 1). We argue that the different propagation speeds are due to the generation of oxygen Frenkel defects [2] in the glowing, pristine phase. In thermal equilibrium, Frenkel defects are extremely unlikely at room temperature. However, the current leads to an overpopulation of short wavelength phonons [3] that is responsible for athermal generation of Frenkel defects.

[1] Mishra, V., Vendrell, X. and Yadav, D., Scripta Mat. **268** (2025) 116877; doi.org/10.1016/j.scripamat.2025.116877
[2] Jongmanns, M. and Wolf, D.E., J. Am. Ceram. Soc. **103** (2020) 589; doi.org/10.1111/jace.16696
[3] Dwedari, M., Brendel, L. and Wolf, D.E., New J. Phys. **24** (2022) 113039; doi.org/10.1088/1367-2630/aca11a

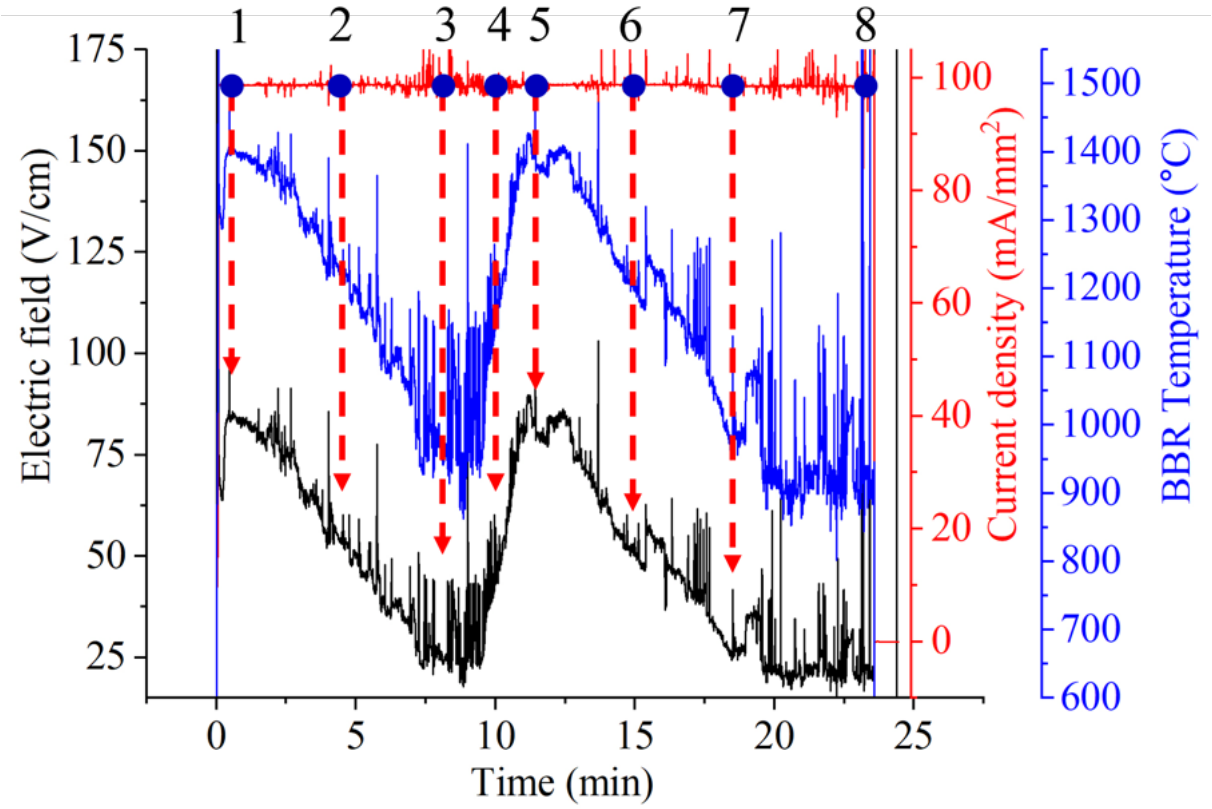

Fig. 1: 1 – 3 and 5 – 7: Conductivity increases while a reduction front passes through the sintered TiO_2 sample held at fixed current in air at room temperature. 4 – 5: Oxidation front runs through the sample. Both reactions start at the cathode and propagate towards the anode. [1]

Notes

$BaTiO_3$ nanoparticle-derived microstructures: sintering approaches and reactivity

Oliver Diwald, Kerstin Neuhauser, Guillem Vives Ollé, Gilles Bourret, Gregor Zickler, and Thomas Berger

Department of Chemistry and Physics of Materials, Universität Salzburg, 5020 Salzburg, Austria

Barium titanate, $BaTiO_3$, is an important material for research and industry.[1] It is widely used in multilayer ceramic capacitors, and due to its outstanding ferroelectric properties, in random-access memories, sensors, or (photo)catalysts. In ceramics the tendency towards miniaturization requires an advanced understanding of property changes that occur while passing from coarse grained the nanosized systems. $BaTiO_3$ nanoparticles that are grown by gas phase synthesis are versatile building blocks for functional microstructures. The organization of the grains at different length scales determines function and performance.[1,2]

We investigated the influence of point defects and spontaneous polarization on $BaTiO_3$ nanoparticle powders that were grown by Flame Spray Pyrolysis.[3] In the next step, corresponding powders were used as starting material and as models to investigate grain growth and characterize the resulting microstructural changes on the surface and inside the nanoparticle layers (Figure 1). We have developed a new polymer-based flash annealing process to produce ceramic monoliths with graded microstructures. New types of surface nano- and microstructures, which originate from layered nanoparticle dispersions or nanoparticle compacts after uniaxial pressing, will be presented.

Microscopy and various spectroscopic techniques (EDX, Raman, UV-Vis Diffuse Reflectance) were used to characterize specific microstructural details of the sintered $BaTiO_3$ surfaces (local grain ensembles, pores, cracks, recrystallized areas, etc.) and to evaluate their influence on charge separation and reactivity towards H_2O, CO_2 and Ag deposition from aqueous solutions. The structural and spectroscopic properties as well as trends in Ag deposition behavior are discussed and compared with coarse-grained structures obtained after application of conventional sintering processes.

This study supports the existence of combined intrinsic and extrinsic size effects in nanocrystalline $BaTiO_3$ ceramics. It contributes to materials science activities that focus on sensors, piezoelectric energy harvesters and for light induced processes functional ceramics.

[1] Buscaglia, V.; Randall, C.A., J. Eur. Ceram. Soc. **40**, (2020) 3744; doi:10.1016/j.jeurceramsoc.2020.01.021;
[2] Diwald, O.; Berger T; Metal Oxide Nanoparticles: Formation, Functional Properties, and Interfaces, **2022** John Wiley & Sons Ltd, doi:10.1002/9781119436782,
[3] Neige, E.; Schwab, T.; Musso, M.; Berger, T.; Bourret, G., R.; Diwald, O.; Small **19** (2023) 2206805; doi.org/10.1002/smll.202206805

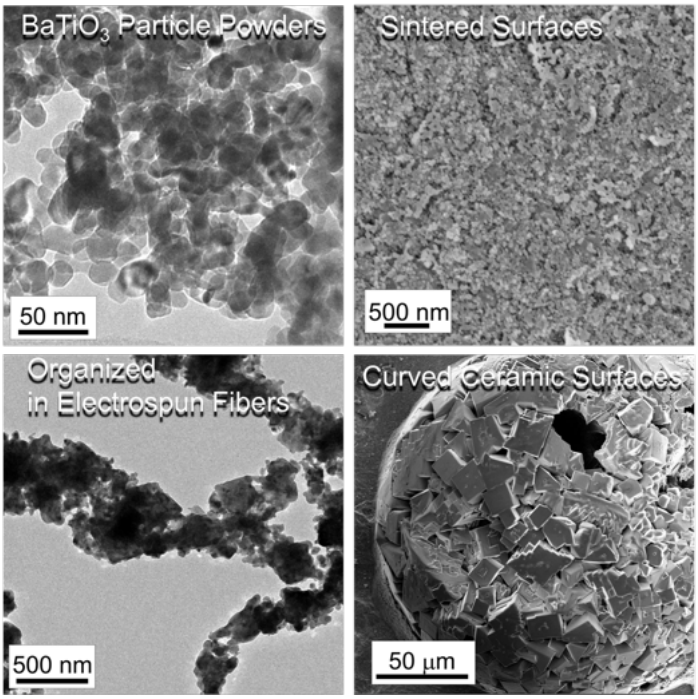

Fig. 1: From gas phase grown $BaTiO_3$ nanoparticles to sintered ceramic surfaces and configurations.

Notes

Machine-learned solute segregation spectra and the stability of nanocrystalline materials

Christopher A. Schuh

Department of Materials Science and Engineering, Northwestern University, Sheridan Road, Evanston, Illinois 60208, USA

It has long been a goal to thermodynamically stabilize nanocrystalline materials through the judicious use of alloying elements that segregate to grain boundaries. Such segregation lowers the excess energy of the interface directly, and also creates deep energetic wells that resist interface migration (and thus grain growth). Historically, designing for grain boundary segregation has been a semi-empirical guessing game, but advances in machine learning have lately opened the door to a rigorous thermodynamic treatment of segregation. This talk will overview the so-called “spectral model” of grain boundary segregation, and the progress in computing large atlases of grain boundary thermodynamic data that are suitable for nanomaterial design on a quantitative basis.

A key feature of segregation spectra in polycrystals is highlighted in Fig. 1, where it is observed that many boundary sites are favorable for solute occupation, but many are also unfavorable. The problem of nanomaterial stability thus amounts to a challenge in finding spectra where the favorable sites outnumber the unfavorable by enough of a margin to reduce the system free energy below that of the competing phase(s), such as the solid solution shown at the right of Fig. 1. With atlases of such spectra now available, stable nanomaterials can be computed directly using CALPHAD-like methodologies. In the finest nanomaterials, one can also explicitly consider the role of higher-order junctions like triple junctions and quadruple nodes, which are also found to have their own segregation spectra and which can materially affect nanomaterial stability.

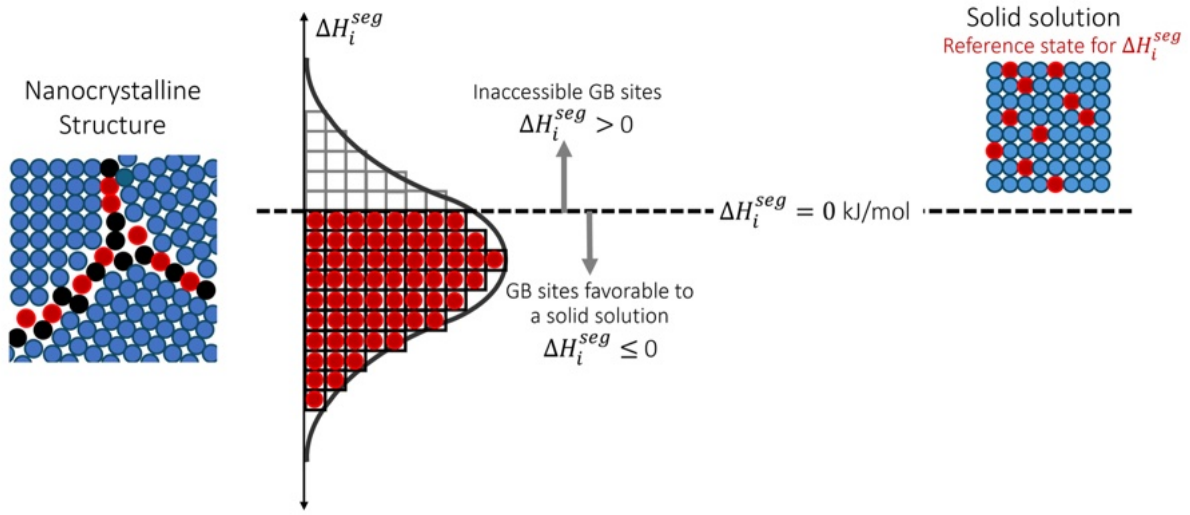

Fig. 1: A schematic illustration of a polycrystal (left) where solutes (red) seek out low energy sites at grain boundaries in a solvent (blue). The spectrum of sites leads to a range of energies (distribution in the middle), and the stability of nanomaterials depends on the fraction of those that are favorable relative to the competing phase(s) like the solid solution shown at the right.

Notes

Synthesis, characterization and structure-property correlations in nanostructured multicomponent, equimolar high entropy oxides

Subramshu S. Bhattacharya[1] and Horst Hahn[2, 3]

1 Nanofunctional Materials Technology Centre (NFMTC), Department of Metallurgical and Materials Engineering, Indian Institute of Technology Madras (IITM), Chennai – 600036, India.
2 Department of Materials Science and Engineering, University of Arizona, Tucson, AZ 85719, USA
3 Institute of Nanotechnology, Karlsruhe Institute of Technology, Karlsruhe, Germany

Multicomponent equimolar oxides (often called high entropy oxides, HEOs) represent a novel class of ceramic materials that exhibit remarkable and often unexpected properties due to their unique compositional diversity that arises from the presence of a multiple number of cations in equimolar proportions on a given sublattice of the crystal structure. These materials have garnered significant attention for their extraordinary room-temperature lithium-ion conductivity, tunable band gaps, colossal dielectric constants, and reversible lithium storage capabilities. The ability to engineer new functionalities by tailoring elemental compositions makes HEOs highly promising for energy storage, optoelectronic applications, and as advanced functional materials.

This study explores different classes of HEOs such as rocksalt, fluorites, perovskites and spinels, involving the presence of 5 or more transition metal and/or rare earth cations. Particular attention is paid to wet chemical methods (such as reverse co-precipitation and the Pechini method) as well as gas-phase synthesis techniques, (including nebulized spray pyrolysis, NSP and flame spray pyrolysis, FSP) for their ability to synthesize high-purity nanostructured HEOs. A comprehensive analysis is conducted on the crystallographic evolution of the different classes of high entropy oxides (HEOs), with a focus on the complex interactions among multiple metal cations that drive the formation of these diverse crystal structures. This study elucidates the interdependence between synthesis conditions, composition, structure and phase stability, and emergent functional properties, offering critical insights for the rational design and optimization of next-generation HEO materials.

Notes

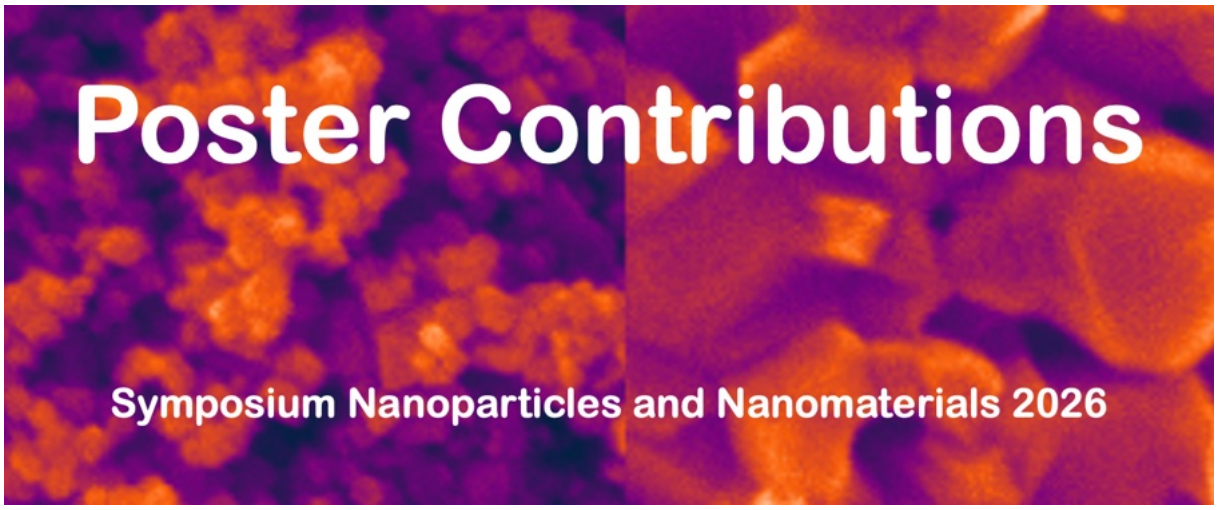

(Abstracts in alphabetical order of the presenting author's last name; presenting author in **bold)**

List of Poster Contributions

Presenting author	Title	Abstract on page	* Order number
Adaköy	Surface-enhanced decomposition of $Al(acac)_3$ in MOCVD	83	5
Menzel	Toward inhalation-relevant in vitro exposure: aerosol-based delivery of nanoparticles at the air-liquid interface	85	1
Peterschik	Robotic synthesis and machine-learning-guided optimization of complex upconverting nanoparticle heterostructures	87	8
Pratali Maffei	From the microscale to the macroscale: kinetic modelling of carbon particles and carbon deposition from methane pyrolysis	89	6
Rahtz	In situ dynamic light scattering during the ultrasonication of nanoparticle dispersions	91	9
Shin	Preparation of polyacrylonitrile-based carbon nanofibers and their applications in energy storage and conversion technologies	93	2
Shkodich	Nanocrystalline CoMnFeNiGa high-entropy alloys across length scales: processing-driven structure and magnetism	95	3
Stepponat	Designing a modular chemical vapor synthesis reactor for in situ X-ray scattering and spectroscopy	97	7
Vukmirović	Entropy-stabilized $LaMnO_3$ based thin films obtained by PAD: structure and transport properties	99	4

*Poster contribution associated with oral presentation; order number assigns board number

(Abstracts in alphabetical order of the presenting author's last name; presenting author in **bold)**

Notes

Surface-enhanced decomposition of $Al(acac)_3$ in MOCVD

Ilyas Adaköy and Burak Atakan

Thermodynamics (EMPI) and Cenide, University of Duisburg-Essen, D-47057 Duisburg, Germany

Aluminum oxide (Al_2O_3) coatings are widely used for corrosion protection and in various other applications such as electrical insulation and surface functionalization. Metalorganic chemical vapor deposition (MOCVD) is a commonly employed technique for the synthesis of Al_2O_3 layers, in which heterogeneous surface reactions and homogeneous gas-phase reactions occur simultaneously. A frequently used precursor is aluminum acetylacetonate ($Al(acac)_3$), owing to its low toxicity and low cost. A detailed understanding of the underlying reaction mechanisms and kinetics is essential for gaining deeper insight into the MOCVD process and for improving the quality of deposited Al_2O_3 coatings. To elucidate the respective roles of gas-phase and surface reactions, a systematic variation of the reactor volume-to-surface (V/A) ratio represents a promising approach.

In this study, the influence of the V/A ratio was investigated in a plug flow reactor using 3D-printed stainless-steel honeycomb structures. This approach enabled an increase of the effective reactor surface area by up to a factor of nine. Honeycomb inserts were pre-conditioned at elevated temperature with $Al(acac)_3$ to obtain Al_2O_3-covered surfaces. In addition, the reactor temperature and gas-phase residence time were varied. The gas-phase composition at the reactor outlet was analyzed by time-of-flight mass spectrometry (TOF-MS) with electron impact ionization; ion intensities were normalized to the Ar signal at the respective condition.

Results show that $Al(acac)_3$ decomposes at significantly lower temperatures in the reactor with increased surface area (honeycomb reactor) compared to an empty reactor without surface enlargement. In the honeycomb reactor, the $Al(acac)_3$ signal falls below the detection limit at 300 °C, whereas in the empty reactor full decomposition occurs only at 400 °C and long residence times. Typical pyrolysis products of $Al(acac)_3$, such as acetone (m/z 58) and acetylacetone (m/z 100), are clearly detected in the honeycomb reactor already at 200 °C. Furthermore, CO_2 (m/z 44) formation is strongly enhanced in the honeycomb reactor, while the signal of acetylacetone decreases at temperatures above 300 °C.

Fig. 1a–b shows the evolution of the normalized intensities of acetylacetone, acetone, and CO_2 as a function of residence time at a reactor temperature of 400 °C. Solid lines represent the honeycomb reactor with increased surface area, while dashed lines correspond to the empty reactor. In the honeycomb reactor, significantly lower acetylacetone intensities are observed compared to the empty reactor, indicating enhanced conversion promoted by the increased surface area. The acetone signal decreases with increasing residence time in the honeycomb reactor, whereas an increasing trend is observed in the empty reactor, suggesting the presence of additional reaction steps in the honeycomb reactor. This interpretation is further supported by the CO_2 (m/z 44) signal, which can be considered a possible end product of the reaction network. CO_2 formation is clearly enhanced in the honeycomb reactor compared to the empty reactor, confirming the stronger conversion of acetone and acetylacetone under increased surface conditions. These observations indicate surface-enhanced pyrolysis of $Al(acac)_3$ and a strong coupling between surface reactions and gas-phase chemistry in MOCVD processes.

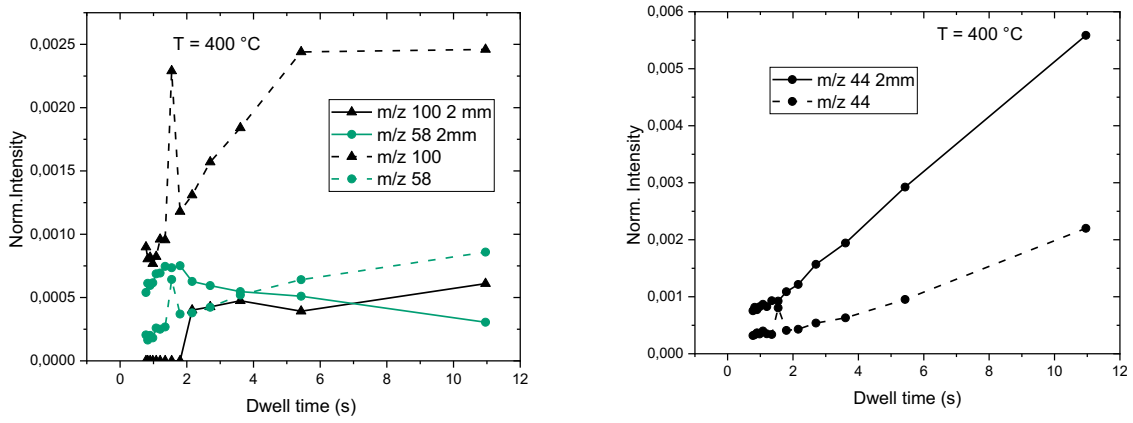

Fig. 1: Evolution of Ar-normalized ion intensities (normalized to the Ar signal) as a function of residence time at 400°C: (a) acetone (m/z 58) and acetylacetone (m/z 100), (b) CO_2 (m/z 44). Solid lines: honeycomb reactor; dashed lines: empty reactor.

Notes

Toward inhalation-relevant in vitro exposure: aerosol-based delivery of nanoparticles at the air-liquid interface

Frank Menzel[3], Merle Küstner[1], Camila Gil Bello[1], Maren Klett[1], Steffen Strehle[2], and Andreas Schober[1]

1 Faculty of Mathematics and Natural Sciences, Technical University of Ilmenau, 98693 Ilmenau, Germany
2 Faculty of Mechanical Engineering, Technical University of Ilmenau, 98693 Ilmenau, Germany
3 Evonik Operations GmbH, EQR Smart Effects, 63457 Hanau, Germany

Nanomaterials exhibit unique physicochemical properties that have led to their rapidly expanding use in research and industrial applications, while simultaneously raising questions about their interactions with biological systems. Inhalation represents a major route of exposure. However, biologically relevant in vitro models remain limited. Due to their small size, nanoparticles can reach the alveolar region of the lung, while deposition efficiency remains limited, as a substantial fraction may be exhaled owing to their low mass. It is therefore crucial for in vitro exposure systems to apply nanoparticles under aerosolized conditions in an air stream to accurately model deposition rates. Beyond less accurate deposition rates, conventional suspension-based exposure approaches may induce changes in the physicochemical properties of nanoparticles prior to interaction with biological systems.

To address these limitations, we present an aerosol-based in vitro exposure approach in which nanoparticles are delivered in an air stream onto cells cultured at the air-liquid interface. The concentration of nanoparticles (AEROSIL® OX 50, AEROSIL® 200 ex) was estimated using a Dustlight measuring device for respirable dust to enable comparative assessment of exposure conditions and to avoid overload.

Preliminary observations suggested localized cellular effects following nanoparticle exposure, as indicated by small clusters of dead cells detected by live/dead staining. Immediately after exposure, the resazurin assay indicated a ~10% decrease in cell viability for both tested nanoparticles, while cell viability recovered after a 24-hour regeneration period.

The presented approach provides a proof-of-concept platform for studying nanoparticle-cell interactions under more inhalation-relevant exposure conditions.

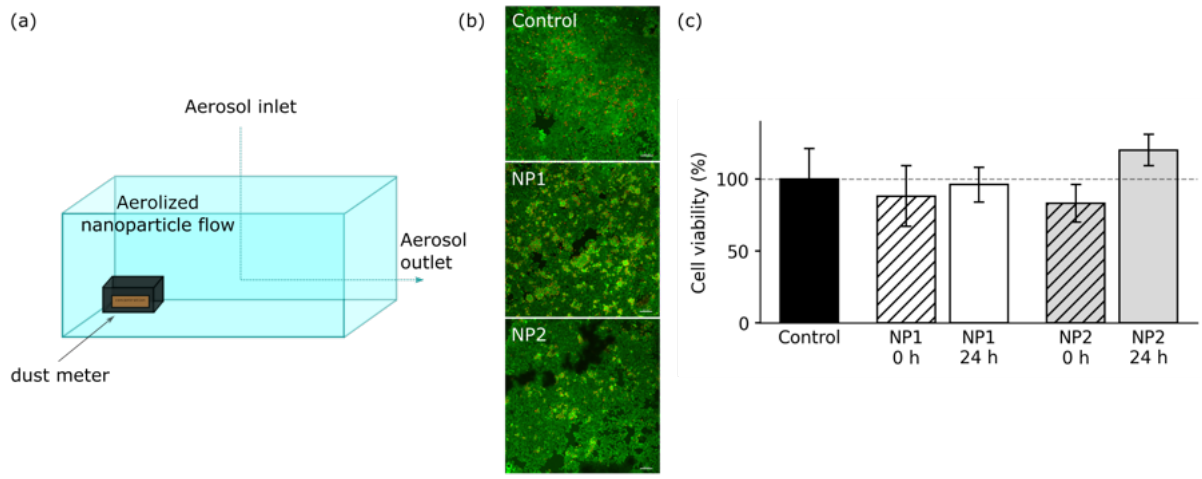

Fig. 1: (a) Schematic illustration of the aerosol-based exposure setup. (b) Representative live/dead staining images acquired immediately after nanoparticle exposure. (c) Quantitative assessment of cell viability using the resazurin assay.

Notes

Robotic synthesis and machine-learning-guided optimization of complex upconverting nanoparticle heterostructures

Hanna Peterschik[1,2], Xiao Qi[1], Sijean Ahn[1], Eric Sivonxay[3], Lucas Attia[3,4], Xiaojing Xia[1], Samuel Blau[3], and Emory Chan[1]

1 Molecular Foundry, Lawrence Berkeley National Laboratory, 94720, USA
2 University of Duisburg-Essen, 47057, Germany
3 Energy Storage and Distributed Resources Division, Lawrence Berkeley National Laboratory, 94720, USA
4 Department of Chemical Engineering, Massachusetts Institute of Technology, 02139, USA

Upconverting nanoparticles (UCNPs) are promising materials for a wide range of applications including biosensing, super-resolution microscopy, and 3D printing, owing to their unique ability to convert low-energy photons into higher-energy emission. However, the design of efficient UCNPs remains challenging due to the complexity of their photophysical networks and their properties are difficult to predict with conventional approaches.

To address this challenge, we developed machine learning models, based on heterogeneous graph neural networks, capable of predicting the optical properties of lanthanide-doped UCNPs based on compositional and structural features. These models predict new compositions with complex, multi-shell heterostructures for UCNPs with up to ten layers and strong blue emission intensities under infrared excitation.

To validate these predictions, we are currently synthesizing a range of ML-optimized multi-layer UCNP heterostructures using an automated synthesis robot and are characterizing their structure and optical properties. Predicted particles with a four-layer architecture could successfully be synthesized.

Notes

From the microscale to the macroscale: kinetic modelling of carbon particles and carbon deposition from methane pyrolysis

Luna Pratali Maffei, L. Giardini, A. Nobili, A. Frassoldati, A. Cuoci, T. Faravelli, and M. Pelucchi

Department of Chemistry, Materials and Chemical Engineering, Politecnico di Milano, Milan, 20133, Italy

Hydrogen (H_2) is a key energy carrier for sustainable development. Pyrolysis of fossil and biogenic hydrocarbons offers a promising short- to mid-term more sustainable alternative to conventional processes (e.g., steam methane reforming) to produce both hydrogen and valuable carbon materials [1]. The economic viability of this process is largely affected by the value of the carbon products formed. In the various reactor technologies under investigation, the decomposition of hydrocarbons is governed by similar chemical kinetics, encompassing gas-phase reactions, aromatic growth, nanoparticle nucleation, and pyrocarbon deposition on surfaces [2], leading to carbon materials with different properties and potential for a wide range of applications (Figure 1a). A robust chemical kinetic model preliminary to computational fluid dynamics simulations can serve as a pivotal tool in guiding reactor design to control energy efficiency and product quality. While the kinetics of methane decomposition is well established, adopting flow reactor technologies with concentrated methane flows with the purpose of carbon material production requires also the modelling of carbon particle formation and carbon deposition on surfaces. Additionally, determining the quality (morphology, mechanical and optical properties) of the carbon formed is key to exploiting this material for different applications.

This work presents the research efforts of CRECK modelling group to build a robust kinetic modelling framework for hydrogen production and carbon materials formation from hydrocarbon pyrolysis (e.g., biomass, plastic waste, fossil fuels) focusing on methane pyrolysis as case of application. The model is built in a modular and hierarchical structure and is refined through iterative validation with kinetic simu-lations of ideal reactor experiments. A novel approach is presented for the modelling of aromatics growth, where reaction rate constants are updated from theoretical calculations and simplified, while consistency among similar species is ensured through automated functional group identification. The solid carbon formation and deposition model is instead improved to include morphological properties of the pyrocarbon, including for instance different aggregation levels in nanoparticles (e.g., different size of primary particles), defect formation in the deposited carbon (e.g., curved zones represented through 5-membered ring species), and carbon deposition on reactor or nanotube walls. Successful applications of the model feature carbon deposition rate from methane pyrolysis in flow reactors, carbon quality of disc brakes reinforced through chemical vapor infiltration, and carbon nanotubes growth rate and purity levels from floating catalyst chemical vapor deposition. A key feature of the model developed herein is the description of the competition between the carbon deposited on the reactor walls and the carbonparticles (soot) formed in the gas phase (Fig. 1b), which allows to explore operating conditions maximizing one or the other product.

[1] C. Giudici, et al., *Adv. Chem. Eng.*, **61**. 1-62. (2023)
[2] F. Serse, et al. *Carbon Trends*, **11**, 100263 (2023)

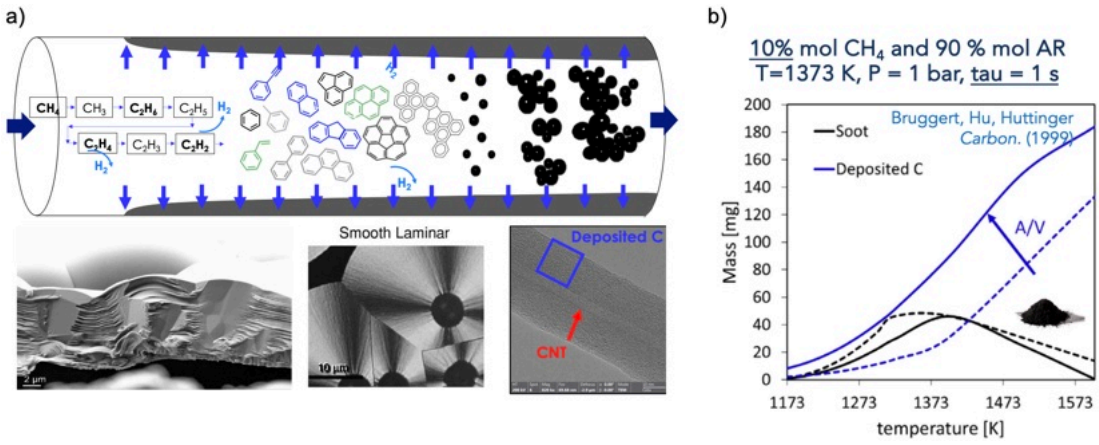

Fig. 1: a) schematic view of pyrocarbon deposition from methane pyrolysis and examples of the type of 123 materials obtained. b) Modeled competition between carbon deposition and soot formation in a flow reactor for methane pyrolysis

Notes

In situ dynamic light scattering during the ultrasonication of nanoparticle dispersions

Robert Rahtz, Markus Winterer, and Martin A. Schroer

Nanoparticle Process Technology, Faculty of Engineering and Center for Nanointegration Duisburg-Essen (CENIDE), University of Duisburg-Essen, 47057 Duisburg, Germany

The application of ultrasound is a frequently used approach to disperse and deagglomerate particles in liquid media. During ultrasonication, the primary cause for particle deagglomeration are cavitation bubbles which, on collapse, send out shock waves and liquid jets that possess sufficient energy to break particle agglomerates apart. As the degree of deagglomeration can affect colloidal stability as well as functional properties of the particles further down the processing line, an understanding of the particle deagglomeration mechanisms is crucial. For this, monitoring the deagglomeration process *in situ* allows to gather further information about the influence of processing on particle properties [1].

In this presentation, we report on *in situ* investigations of nanoparticle dispersions during ultrasonication, combining ultrasound-assisted dispersing with dynamic light scattering (DLS). By this approach, it is possible to continuously follow the development of the particles during ultrasonication with real-time resolution. The potential of *in situ* DLS measurements is demonstrated.

First, the effects of ultrasound on the DLS measurement and the resulting autocorrelation functions (ACFs) and dynamics are discussed (Fig. 1 a)). Then, the capabilities of the setup for tracking the particle size during deagglomeration are presented with titania nanoparticles as an example (Fig. 1 b)).

[1] Mackert, V., Seifert, S. & Winterer, M., Powder Technology **464** (2025) 121227; doi.org/10.1016/j.powtec.2025.121227
[2] Rahtz, R. et al. in preparation

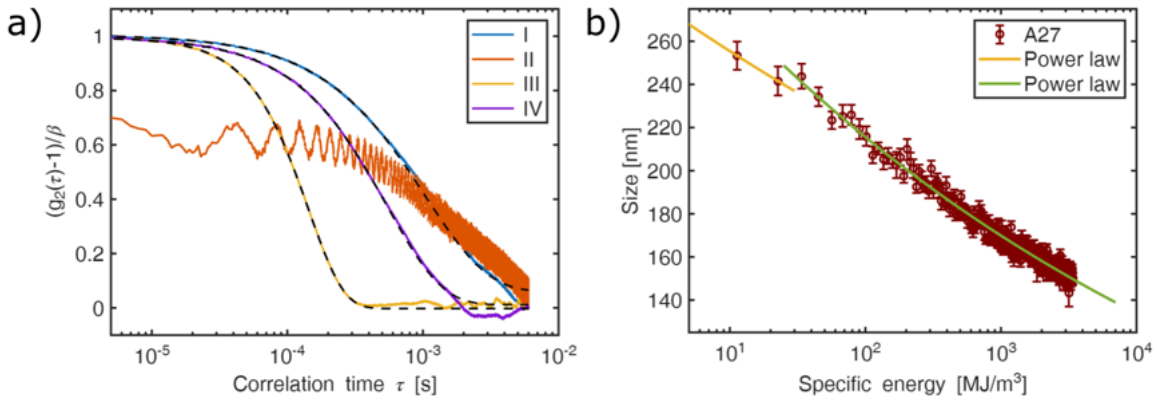

Fig. 1: a): Autocorrelation functions (ACFs) of a titania particle dispersion before ultrasonication (I), during ultrasonication (II), within seconds after ultrasonication (III) and after a few seconds after ultrasonication (IV). b): Size reduction of titania particles as a function of specific energy introduced by ultrasonication [2].

Notes

Preparation of polyacrylonitrile-based carbon nanofibers and their applications in energy storage and conversion technologies

Eui-Young Shin[1,2], Muhammad Saif Maqsood[2], Wael Ali[1,2], Andreas Wego[3], Thomas Mayer-Gall[1,2], and Jochen S. Gutmann[1,2]

1 German Textile Research Center North-West, 47798 Krefeld, Germany
2 Department of Physical Chemistry, University of Duisburg-Essen, 45141 Essen, Germany
3 Industrievereinigung Chemiefaser e.V., 60329 Frankfurt am Main, Germany

Carbon nanofibers (CNFs), synthesized through the electrospinning of Polyacrylonitrile (PAN) polymer, have emerged as a significant class of nanomaterials, drawing significant attention in advanced materials research. The electrospinning technique allows for precise engineering of nanofiber structures, enabling the tailoring of properties such as high surface area, mechanical strength, and electrical conductivity. PAN-fibers are spun into nonwoven PAN nanofibers via electrospinning technique and then converted to CNFs through stabilization process under air conditions, followed by carbonization at elevated temperatures under a continuous flow of nitrogen gas. [1,2]

The resulting CNFs exhibit high specific surface area, excellent conductivity, and robust mechanical strength. Furthermore, these CNFs can be easily modified by incorporating sacrificial polymers into the spinning solution to increase specific surface area or directly embedding nanoparticles to enhance conductivity. These properties make CNFs well-suited for use in energy storage and conversion technologies, such as supercapacitors, lithium-sulfur batteries and fuel cells (Fig.1).

In supercapacitors, CNFs serve as free-standing efficient electrode materials, enabling high energy densities and rapid charge-discharge cycles due to their large surface area and inherent redox-active nanoparticles. In lithium-sulfur batteries, CNFs enhance the electrical conductivity of the sulfur cathode, improving battery performance. Their high surface area allows for better sulfur utilization, increasing capacity and energy density while also trapping polysulfides to reduce the shuttle effect and enhance cycle life and stability. In fuel cells, CNFs demonstrate high catalytic activity and electrical conductivity when platinum nanoparticles are integrated on the surface of the nanofibers, resulting in improved energy efficiency and performance. [1] The production method presented and remarkable properties of PAN-based CNFs offer promising avenues for the development of advanced materials for various energy-related applications.

[1] Xue, J.; Wu, T.; Dai, Y.; Xia, Y. Electrospinning and Electrospun Nanofibers: Methods, Materials, and Applications. Chemical reviews (2019), **119**, 5298–5415; doi.org/10.1021/acs.chemrev.8b00593
[2] Islam, M. S.; Ang, B. C.; Andriyana, A.; Afifi, A. M. A review on fabrication of nanofibers via electrospinning and their applications. SN Appl. Sci. **2019**, 1; doi.org/10.1007/s42452-019-1288-4

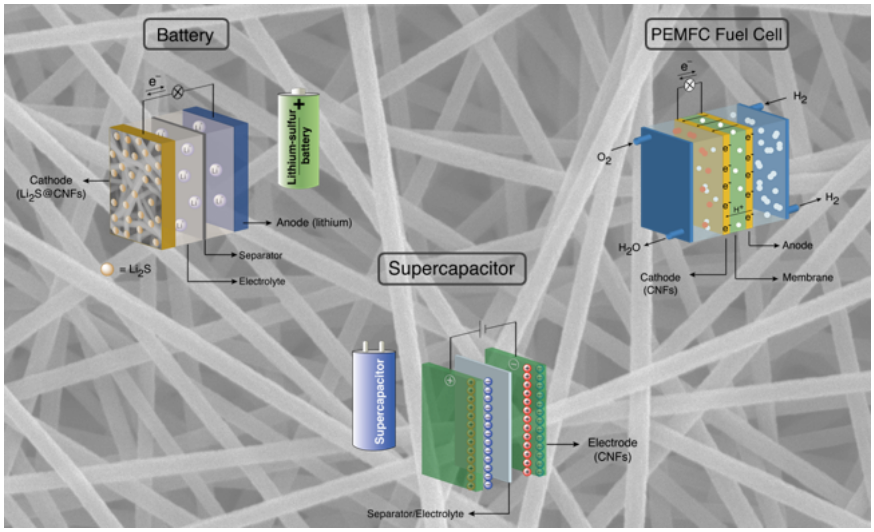

Fig. 1: Electrospun nanofiber nonwoven in the background illustrating their use as versatile functional scaffolds for electrochemical energy technologies. Schematic application examples include a battery, a supercapacitor, and a proton-exchange membrane fuel cell.

Notes

Nanocrystalline CoMnFeNiGa high-entropy alloys across length scales: processing-driven structure and magnetism

Natalia F. Shkodich[1], T. Smoliarova[1], V. Nallathambi[2,3], L.M. Feitosa[3], E. Adabifiroozjaei[4], I. Tarasov[1], H. Shokri[5], B. Gault[3], S. Reichenberger[2], L. Molina-Luna[4], B. Gökce[5], S. Barcikowski[2], and M. Farle[1]

1 Faculty of Physics and Center of Nanointegration (CENIDE), University of Duisburg-Essen, 47057 Duisburg, Germany
2 Technical Chemistry I and Center of Nanointegration (CENIDE), University of Duisburg-Essen, 45141 Essen, Germany
3 Max Planck Institute for Sustainable Materials, Max-Planck-Str.1, 40237 Düsseldorf, Germany
4 Department of Materials and Geosciences, TU Darmstadt, Peter-Grünberg-Str. 2, Darmstadt 64287, Germany
5 School of Mechanical Engineering and Safety Engineering, University of Wuppertal, 42119 Wuppertal, Germany

High-entropy alloys (HEAs) have garnered significant attention due to their unique synergy of structural, physical, chemical, and magnetic properties arising from their multiprincipal element design [1]. In magnetic HEAs, the balance between ferromagnetic (Fe, Co, Ni) and antiferromagnetic (Mn) interactions, together with phase constitution and microstructure, governs the resulting magnetic behavior [1-3]. The incorporation of Ga as an *sp*-element modifies magnetic ordering and phase stability; however, its low melting point (T_m = 302.9 K) complicates conventional melting-based synthesis, often resulting in compositional inhomogeneity and coarse microstructures. Consequently, Ga-containing magnetic HEAs have been mainly studied in conventionally processed bulk form, while nanocrystalline bulk, powder, and nanoparticle forms remain largely unexplored. Nanocrystallinity offers an additional degree of freedom to tailor phase stability, magnetic exchange interactions, and functional properties via enhanced grain-boundary and size effects.

In this study, we successfully demonstrate the controlled synthesis of CoMnFeNiGa HEAs in three distinct nanocrystalline forms [3]: bulk, micronsized powders (MPs), and nanoparticles (NPs). Compositionally homogeneous, single-phase *FCC*, nanocrystalline (8 nm) MPs (Fig.1a-c) were produced by short-term (190 min) high-energy ball milling (HEBM), enabling the incorporation of low melting Ga into a stable HEA matrix. Subsequent SPS induces partial *FCC→BCC* transformation and nanoscale compositional segregation. Laser fragmentation in liquids (LFL) enables the production of HEA NPs with two morphologies (spheres and quasi-2D platelets) in a single step, directly from the HEBM MPs. All three types of HEAs exhibit soft ferromagnetic behavior at RT with saturation magnetization (M_s) of 19.5–33.5 Am²/kg for MPs and NPs, while the M_s of bulk material is 2–4 times larger (88.8 Am²/kg). A short thermal treatment (1000 K, 30 s) significantly enhanced M_s and increased the Curie temperature of the MPs to 105.6 Am²/kg (by 272%) and 785 K, of the NPs to 46.9 Am²/kg (by 44.3%) and 850 K, and of the bulk material to 106 Am²/kg (by 44.3%) and 793 K. This enhancement is associated with structural and compositional changes, as observed by in-situ TEM heating and temperature-dependent XRD [3]. Additionally, SPS-consolidated HEA bulk derived from HEA MPs exhibits a Vickers hardness of $HV_{0.2}$ = 6 GPa, nearly six times higher than that of bulk material consolidated from elemental powders.

[1] Han, L., et al., Adv. Mater. **33** (2021) 2102139; doi.org/10.1002/adma.202102139.
[2] Shkodich, N. F., et al., Acta Mater. **284** (2025) 120569; doi.org/10.1016/j.actamat.2024.120569.
[3] Shkodich, N. F., et al., Faraday Discuss. (2025); doi.org/10.1039/D5FD00080G.

Financial support from the DFG, CRC/TRR 270 (project ID 405553726), and DFG FA209/27-1 is acknowledged.
VN, SB, BG thank International Max-Planck Research School (IMPRS-SurMat/SusMet)

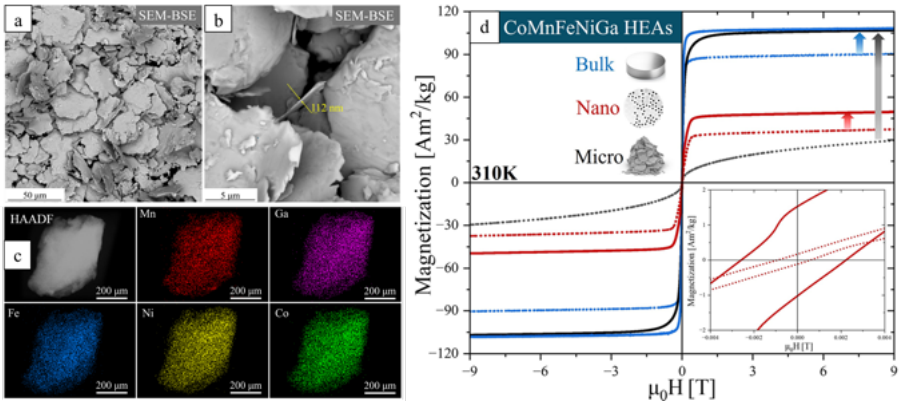

Fig. 1: CoMnFeNiGa HEA MPs: (a) and (b) SEM images with different magnifications; (c) STEM image with EDX mapping of the elements; (d) Field-dependent magnetization *M*(H) at 310 K before (dashed) and after (solid) heat treatment (-9T > B_{ext} > 9T) of HEA NPs (red), MPs (black) and bulk (blue).

Notes

Designing a modular chemical vapor synthesis reactor for *in situ* X-ray scattering and spectroscopy

Max Stepponat, Shradha R. Joshi, and Markus Winterer

Nanoparticle Process Technology, Universität Duisburg-Essen, 47057 Duisburg, Germany

Chemical vapor synthesis (CVS) is a method for the production of nanoparticles (NP) with highly desired particle characteristics such as high specific surface area and crystallinity. The properties of NP may be controlled and optimized by adjusting the CVS process parameters. In a conventional CVS process, a precursor material is evaporated and introduced into a heated, tubular flow channel under reduced pressure with the aid of a carrier gas. There, the precursor material interacts with reactants to form NP. Little is known about the actual NP formation and growth mechanisms in CVS. One way to study the formation of the nanoparticles is to use *in situ* small-angle X-ray scattering (SAXS), wide-angle X-ray scattering (WAXS) and X-ray absorption fine structure spectroscopy (XAFS) using high-energy X-rays at synchrotron radiation facilities. For this purpose, a modular and customizable CVS reactor with the possibility of *in situ* investigation is developed.

The basic setup (Fig. 1) consists of a water-cooled vacuum vessel inside which an Al_2O_3 tube is used as a reactor. The process temperature is achieved by inductive heating. The susceptor is placed concentrically around the tube. The length of the susceptor is variable which enables a fast variation of the most important process parameter – the temperature-time profile – independent of other parameters. The vacuum vessel consists of several segments. The bottom flange consists of the inlets for precursor, reactant and flushing gas and is heated or cooled depending on the precursor material. The two segments on top have feedthroughs for the HF power supply and temperature measurement using a pyrometer. The head segment provides four vacuum tight, X-ray transparent windows for the introduction and observation of hard X-rays to observe SAXS, WAXS and XAFS. The top flange has an outlet which connects the entire CVS reactor to a vacuum pump including total process pressure control (Fig. 2). The operation of the system has been demonstrated by some studies at DESY (e.g. The formation of tin oxide nanoparticles studied by SAXS, and the formation of iron oxide nanoparticles investigated by X-ray absorption spectroscopy (XAS)) [1].

Here, we describe the design and modification of a mobile CVS reactor that facilitates operation at synchrotron radiation facilities, enhances X-ray detection capabilities, and allows the application of additional characterization techniques for elucidating nanoparticle formation and growth mechanisms in CVS.

[1] Schroer, M. A. Levish, A. Yildizlar, Y. Stepponat, M., and Winterer, M., Rev. Sci. Instrum. **93** (2022) 113706; doi: 10.1063/5.0122461

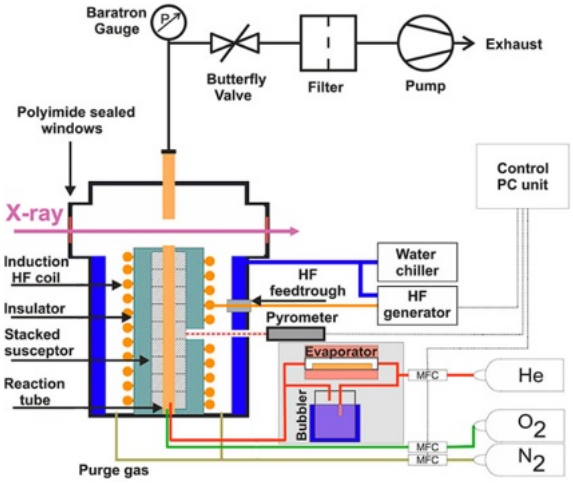

Fig. 2: Scheme of the CVS set-up [1]

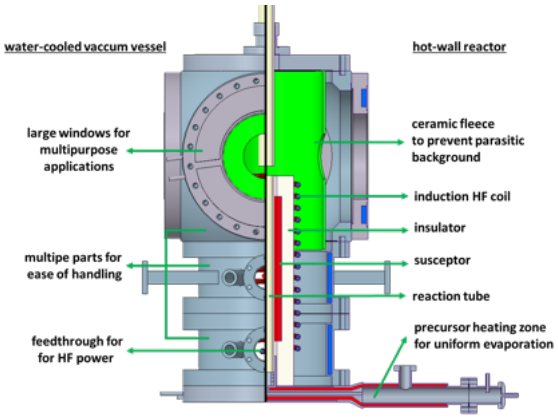

Fig. 3: Concept diagram of the improved CVS reactor

Notes

Entropy-stabilized $LaMnO_3$ based thin films obtained by PAD: structure and transport properties

Jelena Vukmirović[1], Danica Piper[2], Iva Toković[1], Xuyun Guo[3], Felipe Morgado[4], Bojan Miljević[1], Sara Joksović[2], Ivan Stijepović[1], Marija Milanović[1], and Vladimir V. Srdić[1,5]

1 Department of Materials Engineering, Faculty of Technology Novi Sad, University of Novi Sad, Bul. Cara Lazara 1, 21000 Novi Sad, Serbia
2 Institute BioSense, University of Novi Sad, Dr. Zorana Đinđića 1, Novi Sad, Serbia
3 School of Chemistry, Centre for Research on Adaptive Nanostructures and Nanodevices (CRANN) and Advanced Materials Bio-Engineering Research Centre (AMBER), Trinity College Dublin, D02 PN40 Dublin, Ireland
4 Nanoparticle Process Technology, Faculty of Engineering, University Duisburg Essen, Lotharstr. 1, 47057 Duisburg, Germany
5 Serbian Academy of Sciences and Arts, Kneza Mihajla 35, 11000 Belgrade, Serbia

Functional oxide thin films play important role in nanoscale electronics due to the wide spectra of properties that can be tuned by composition and strain design. Vapor deposition techniques were standard in deposition of epitaxial functional thin films for years. Challenging procedure which includes expensive equipment with high-vacuum system hindered development of mentioned techniques for complex oxide thin films production at the large scale. Recently, chemical solution deposition (CSD) techniques were considered as good alternative for overcoming these limitations and enabling cost-effective and scalable preparation of epitaxial complex oxide thin films. Possibility of producing high quality functional epitaxial perovskite thin films by CSD polymer assisted deposition technique was investigated in this work.

Epitaxial $LaMnO_3$ based thin films were prepared by polymer assisted deposition (PAD) technique in combination with spin coating. A systematic investigation was conducted by progressively increasing the number of A-site cations (from one up to five: La^{3+}, Sr^{2+}, Ca^{2+}, Sm^{3+} and Ba^{2+}/Ce^{3+}) in the ABO_3 structure to explore the entropy-driven stabilization of single-phase perovskite structures under epitaxial strain. All samples were prepared by dissolving the corresponding nitrates in water using PEI and EDTA as stabilizing agents. Prepared solutions were deposited at previously cleaned $SrTiO_3$ (001) single crystal substrates and thermally treated up to 900 °C to obtain epitaxial thin films. Structural analyses of films performed by XRD and HRTEM, confirmed highly oriented growth of $LaMnO_3$ based thin films. Additionally, electrical behavior of films was observed by resistivity measurements in wide range of temperatures (-100 to 300 °C).

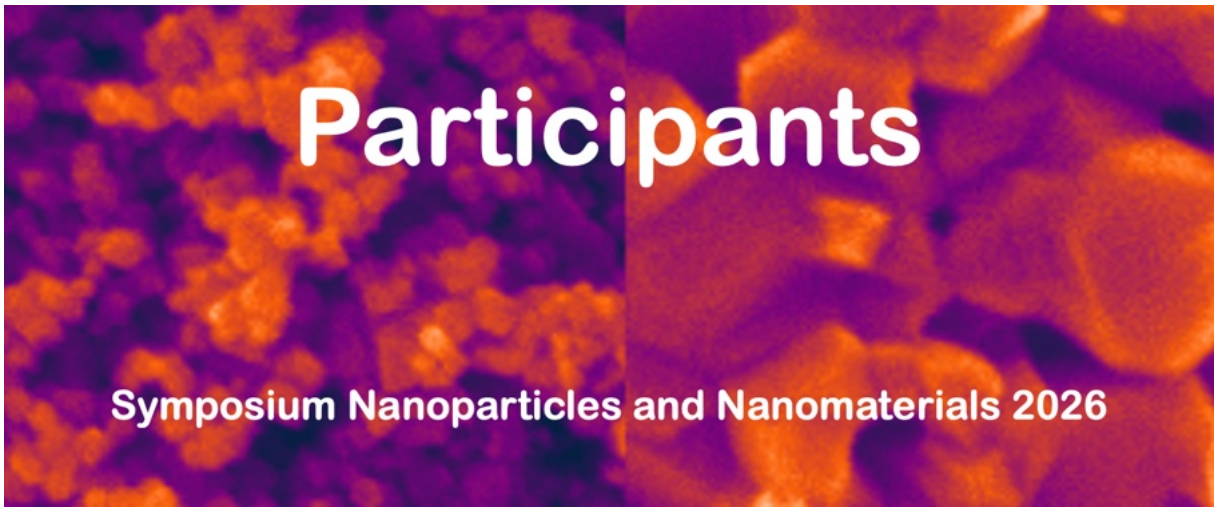
Participants
Symposium Nanoparticles and Nanomaterials 2026

Participants – 1

Name	affiliation	email	country	page
Adaköy, Ilyas	Universität Duisburg-Essen	ilyas.adakoey @uni-due.de	Germany	51, 83
Anselmi-Tamburini, Umberto	Università di Pavia	tau @unipv.it	Italia	19, 45
Atakan, Burak	Universität Duisburg-Essen	burak.atakan @uni-due.de	Germany	51, 83
Bacher, Gerd	Universität Duisburg-Essen	gerd.bacher @uni-due.de	Germany	27, 37
Bhattacharya, Sarbari	Bangalore University	sarbari.bhattacharya @bub.ernet.in	India	21
Bhattacharya, Subramshu S.	Indian Institute of Technology Madras	ssb @iitm.ac.in	India	77
Boies, Adam	Stanford University	aboies @stanford.edu	USA	59
Chan, Emory	Lawrence Berkeley Laboratory	EMChan @lbl.gov	USA	25, 87
Deimel, Sabine	Universität Duisburg-Essen	sabine.deimel @uni-due.de	Germany	
Diwald, Oliver	University of Salzburg	oliver.diwald @plus.ac.at	Austria	73
Fidelus, Janusz	Jan Kochanowski University	janusz.fidelus @ujk.edu.pl	Poland	47
Gladfelter, Wayne L.	University of Minnesota	wlg @umn.edu	USA	29
Joshi, Shradha R.	Universität Duisburg-Essen	shradha.joshi @uni-due.de	Germany	43, 97
Kruis, F. Einar	Universität Duisburg-Essen	einar.kruis @uni-due.de	Germany	65
Kümmell, Tilmar	Universität Duisburg-Essen	tilmar.kuemmell @uni-due.de	Germany	37
Lorke, Axel	Universität Duisburg-Essen	axel.lorke @uni-due.de	Germany	55, 57
Maier, Joachim	Max Planck Institute for Solid State Research	office-maier @fkf.mpg.de	Germany	11

Participants – 2

Name	affiliation	email	country	page
Menzel, Frank	Evonik Operations GmbH	frank.menzel.@evonik.com	Germany	23, 85
Morgado de Oliveira, Felipe F.	Universität Duisburg-Essen	felipe.fmorgado@uni-due.de	Germany	13 53, 99
Münzer, Franziska	Universität Duisburg-Essen	franziska.muenzer@uni-due.de	Germany	39
Peterschik, Hanna	Universität Duisburg-Essen	hanna.peterschik@stud.uni-due.de	Germany	87
Pratali Maffei, Luna	Politecnico di Milano	luna.pratali@polimi.it	Italia	33, 89
Pratsinis, Sotiris E.	ETH Zürich	sotiris.pratsinis@ptl.mavt.ethz.ch	Switzer-land	49
Rahtz, Robert	Universität Duisburg-Essen	robert.rahtz@stud.uni-due.de	Germany	91
Schleberger, Marika	Universität Duisburg-Essen	marika.schleberger@uni-due.de	Germany	35
Schleife, André	University of Illinois at Urbana-Cham-paign	schleife@illinois.edu	USA	31
Schroer, Martin A.	Universität Duisburg-Essen	martin.schroer@uni-due.de	Germany	17, 39, 43, 45, 69, 91
Schuh, Christopher A.	Northwestern Univer-sity	schuh@northwestern.edu	USA	75
Schulte, Jeldrik	Universität Duisburg-Essen	jeldrik.schulte@uni-due.de	Germany	69
Schulz, Christof	Universität Duisburg-Essen	christof.schulz@uni-due.de	Germany	61
Shin, Eui-Young	Deutsches Textilfor-schungszentrum Nord-West gGmbH	shin@dtnw.de	Germany	93
Shkodich, Natalia	Universität Duisburg-Essen	natalia.shkodich@uni-due.de	Germany	95
Siebecke, Katja	Universität Duisburg-Essen	katja.siebecke@uni-due.de	Germany	17
Srdić, Vladimir V.	University Novi Sad	srdicvv@uns.ac.rs	Serbia	13, 99

Participants – 3

Name	affiliation	email	country	page
Stepponat, Maximilian	Universität Duisburg-Essen	maximilian.stepponat@uni-due.de	Germany	97
Todd, Richard I.	University of Oxford	richard.todd@materials.ox.ac.uk	United Kingdom	67
Villanova, Julie	European Synchrotron Radiation Facility	julie.villanova@esrf.fr	France	41
Vukmirović, Jelena	University Novi Sad	jelenavukmirovic1@gmail.com	Serbia	13, 99
Wiggers, Hartmut	Universität Duisburg-Essen	hartmut.wiggers@uni-due.de	Germany	61, 63
Winterer, Markus	Universität Duisburg-Essen	markus.winterer@uni-due.de	Germany	39, 43, 53, 69, 91, 97
Wöhrl, Nicolas	Universität Duisburg-Essen	nicolas.woehrl.@uni-due.de	Germany	55, 57
Wolf, Dietrich E.	Universität Duisburg-Essen	dietrich.wolf@uni-due.de	Germany	71
Yildiz, Bilge	Massachusetts Institute of Technology	byildiz@mit.edu	USA	15

Back Cover Acknowledgement
The inside and outside back cover images have been generated using data from OpenStreetMap (https://www.openstreetmap.org/) published under ODbL and ACTV (https://actv.avmspa.it/).

Travel to and from San Servolo

LINEA 20 **S.MARCO/S.ZACCARIA - S.SERVOLO - S.LAZZARO - S.SERVOLO - S.MARCO/S.ZACCARIA**

IN VIGORE DAL 01 APRILE 2022

LIDO S.M.E. "E"				06:10											16:00				18:35										
S.MARCO-S.ZACCARIA "B"	06:55	07:15	08:10	-	08:40	09:00	09:20	09:50	10:30	11:10	11:50	12:30	13:10	13:50	14:30	15:10	15:40	-	16:30	17:10	17:50	18:10	-	18:10	19:50	20:30	21:30	22:30	23:30	00:30
S.SERVOLO	07:05	07:25	08:20	08:20	08:50	09:10	09:30	10:00	10:40	11:20	12:00	12:40	13:20	14:00	14:40	15:20	15:50	-	16:40	17:20	18:00	18:20	-	19:20	20:00	20:40	21:40	22:40	23:40	00:40
S.LAZZARO	-	07:30	08:25	-	-	-	09:35	-	10:45	-	12:05	-	13:25	-	14:45	15:25	-	-	16:45	17:25	-	18:25	-	-	-	-	-	-	-	-
S.SERVOLO	-	07:35	08:30	-	-	-	09:40	-	10:50	-	12:10	-	13:30	-	14:50	15:30	-	-	16:50	17:30	-	-	-	18:45	-	-	-	-	-	-
S.MARCO-S.ZACCARIA "B"	07:15	07:45	08:40		09:00	09:20	09:50	10:10	11:00	11:30	12:20	12:50	13:40	14:10	15:00	15:40	-	16:20	17:00	17:40	18:10	-	18:55	19:30	20:10	20:50	21:50	22:50	23:50	00:50
LIDO S.M.E. "E"																	16:00					18:35								

(A) = FERMA A S.LAZZARO SOLO SU RICHIESTA DEI PASSEGGERI, MENTRE L'IMBARCO SI PUÒ PRENOTARE TELEFONANDO, ALMENO 20 MINUTI PRIMA, AL NUMERO VERDE 800845065

San Servolo


VIU Front Office
Boat Stop
ACTV Linea 20
Main Entrance
Hotel Reception
Conference Hall
Aula Magna (1st floor)
Bar - Café
Fondazione Franca e Franco Basaglia
Sala Basiglia for Conference Dinner
Residential Hall
Residential Hall
San Servolo
Residential Hall
Residential Hall
Sports Grounds
Restaurant
Restaurant